universität wien

MASTERARBEIT / MASTER'S THESIS

Titel der Masterarbeit / Title of the Master's Thesis

„ An inducible dual-guide CRISPR/Cas9 approach resolves the cellular assembly and functions of mammalian RNA exosome subunits "

verfasst von / submitted by

Nikolaus Beer, BSc

angestrebter akademischer Grad / in partial fulfilment of the requirements for the degree of

Master of Science (MSc)

Wien, 2022 / Vienna, 2022

Studienkennzahl lt. Studienblatt / degree programme code as it appears on the student record sheet:	UA 066 834
Studienrichtung lt. Studienblatt / degree programme as it appears on the student record sheet:	Masterstudium Molekulare Biologie UG2002
Betreut von / Supervisor:	Univ.-Prof. Dr. Stefan Ameres

1 Table of Contents

1 Abstract

The RNA exosome is an evolutionary conserved 3′ to 5′exoribonuclease multi-subunit complex involved in the processing and/or degradation of almost every class of RNA to sustain organismal viability. In eukaryotes, the RNA exosome is composed of a catalytically inert core that consists of nine unique subunits (Exosc1-9) which have been proposed to form an essential scaffold for RNA processing and decay mediated by associated exoribonucleases of the Dis3-family (Dis3 in the nucleus and Dis3L in the cytoplasm) and Exosc10 (in the nucleolus). While the structure of the RNA exosome and many of its molecular substrates have been extensively studied, a comprehensive view on the physiological and molecular function of individual core complex components as well as their cellular assembly remains poorly understood. This is not least due to the lack of experimental systems that allow to systematically interfere with essential protein components at timescales that account for detrimental downstream consequences.

Here, I established a doxycycline-inducible dual-guide CRISPR/Cas9 approach in mouse embryonic stem cells that enables the systematic parallel depletion of essential gene products at timescales that expose direct molecular and phenotypic consequences. By comprehensively applying this experimental strategy to individual components of the RNA exosome and combining it with cell growth competition assays, I confirmed the essential function of most complex constituents except for the peripheral component Exosc1. In fact, RNA sequencing revealed that the degradation of promoter upstream transcripts (PROMPTs) – transcriptional byproducts that are degraded by the nuclear RNA exosome – were substantially less dependent on Exosc1 when compared to all other core components, suggesting that Exosc1 is at least partially dispensable for RNA exosome function. Finally, I performed systematic quantitative Western blot analyses to assess the co-destabilization of exosome components, which revealed a cellular hierarchy of RNA exosome complex formation. In contrast to a previously proposed model that suggested the involvement of pre-formed dimers, my observations strongly support a sequential assembly model, which relies on the initial association of a core-trimer consisting of Exosc2, 4 and 7, followed by the stepwise recruitment of Exosc7, 8, 9, 5 and 3. Notably, the formation of such an RNA exosome octameric core is required to stabilize the cytoplasmic catalytic component Dis3L but not its nuclear counterpart Dis3. Consistent with the phenotypically dispensable role of Exosc1, its association with the RNA exosome octameric core is merely required to stabilize the nuclear exoribonuclease Exosc10 and determining its role in RNA exosome function warrants further investigation.

In summary, this thesis establishes a novel experimental strategy for time-resolved loss-of-function assays of essential genes in mouse embryonic stem cells, establishing Exosc1 as a partially dispensable and peripheral component of the otherwise essential RNA exosome core complex and revealing unprecedented insights into the cellular assembly of the RNA exosome.

Keywords: RNA degradation, RNA processing, in vivo protein complex assembly, RNA exosome, CRISPR/Cas9 genome engineering

2 Zusammenfassung

Das RNA-Exosom ist ein evolutionär konservierter 3′-5′-Exoribonuklease-Komplex mit mehreren Untereinheiten, der an der Verarbeitung und/oder dem Abbau fast aller RNA-Klassen beteiligt ist, und für das Überleben von Organismen essenziell ist. In Eukaryonten besteht das RNA-Exosom aus einem katalytisch inerten Kern, der aus neun einzigartigen Untereinheiten (Exosc1-9) besteht. Der Kern dient als wesentliches Gerüst für die RNA-Verarbeitung und den RNA-Abbau, was durch assoziierte Exoribonukleasen der Dis3-Familie (Dis3 im Zellkern und Dis3L im Zytoplasma) und Exosc10 (im Nukleolus) bewerkstelligt wird. Während die Struktur des RNA-Exosoms und viele seiner molekularen Substrate eingehend untersucht wurden, ist ein umfassender Überblick über die physiologische und molekulare Funktion der einzelnen Komponenten des Komplexes sowie der intrazellulären Assemblierung nach wie vor kaum bekannt. Dies liegt nicht zuletzt daran, dass es an experimentellen Systemen mangelt, die es erlauben, systematisch in essenzielle Proteinkomponenten einzugreifen, welche schädliche nachgelagerte Konsequenzen berücksichtigen.

Hier habe ich einen Doxycyclin-induzierbaren Dual-Guide-CRISPR/Cas9-Ansatz in embryonalen Stammzellen der Maus etabliert, der das systematische parallele Ausschalten essenzieller Genprodukte in Zeitskalen ermöglicht, welche direkte molekulare und phänotypische Konsequenzen aufzeigen. Durch die umfassende Anwendung dieser experimentellen Strategie auf einzelne Komponenten des RNA-Exosoms und in Kombination mit Zellwachstumskonkurrenz-Assays konnte ich die essenzielle Funktion von Komplexbestandteile bestätigen, mit Ausnahme der peripheren Komponente Exosc1. Tatsächlich ergab die RNA-Sequenzierung, dass der Abbau von Promoter-Upstream-Transkripten (PROMPTs) - Transkriptionsnebenprodukte, die vom nukleären RNA-Exosom abgebaut werden - im Vergleich zu allen anderen Kernkomponenten deutlich weniger von Exosc1 abhängig war, was darauf hindeutet, dass Exosc1 für die Funktion des RNA-Exosoms zumindest teilweise entbehrlich ist. Schließlich führte ich systematische quantitative Western-Blot-Analysen durch, um die Co-Destabilisierung von Exosom-Komponenten zu messen, wodurch die zelluläre Hierarchie der RNA-Exosom-Komplexbildung aufzeigt werden konnte. Im Gegensatz zu einem früher vorgeschlagenen Modell, das die Beteiligung von vorgebildeten Dimeren nahelegt, sprechen meine Beobachtungen für ein sequenzielles Assemblierungsmodell, das auf der anfänglichen Assoziation eines Trimers, bestehend aus Exosc2, 4 und 7, beruht, gefolgt von der schrittweisen Rekrutierung von Exosc7, 8, 9, 5 und 3. Bemerkenswert ist, dass die Bildung eines solchen oktameren RNA-Exosom-Kerns erforderlich ist, um die zytoplasmatische katalytische Komponente Dis3L zu stabilisieren, nicht aber ihres nuklearen Gegenstücks Dis3. Im Einklang mit der phänotypischen Entbehrlichkeit von Exosc1 ist dessen Assoziierung mit dem oktameren Kern des RNA-Exosoms lediglich zur Stabilisierung der nukleären Exoribonuklease Exosc10 erforderlich. Eine Klärung der Rolle von Exosc1 in der Funktion des RNA-Exosoms bedarf damit weiterer Nachforschungen.

Zusammenfassend wurde mit dieser Arbeit eine experimentelle Strategie für zeitaufgelöste Loss-of-Function-Tests von essenziellen Genen in murinen Stammzellen etabliert, durch welche Exosc1 als teilweise entbehrliche und periphere Komponente des ansonsten essenziellen RNA-Exosom-Kernkomplexes dargestellt und noch neue Einblicke in die zelluläre Assemblierung des RNA-Exosoms offenbart werden konnten.
Schlüsselwörter: RNA Abbau, RNA Prozessierung, in vivo Protein-Komplexbildung, RNA-Exosom, CRISPR/Cas9 Genom-Editierung

3 Introduction

RNA molecules fulfill a plethora of essential functions in all living cells. The functional and structural diversity of RNA molecules demands well-coordinated post-transcriptional modulation. This is in part executed by the RNA exosome, an evolutionary conserved 3′ to 5′ exoribonuclease complex, that is involved in the processing and/or degradation of nearly all classes of RNA (1).

In eukaryotes, the core of the RNA complex is catalytically inert, however all nine core subunits are thought to be essential, as is the case in *S. cerevisiae* and *S. pombe* (2–6). While the structure of the exosome has been resolved, little is known about the assembly process (7). In fact, the roles of individual subunits in complex assembly and function remain largely elusive.

3.1 Structural basis and evolutionary conservation of major 3′ to 5′ exoribonucleolytic machineries

3′ to 5′ RNA decay is a process conserved in all three kingdoms of life with shared mechanistic and structural features between the enzymes catalyzing RNA decay (1,7). In eukaryotes this function is carried out in both in the nucleus and cytoplasm by a multi-subunit complex, known as the RNA exosome (8,9).

The overall structure of the RNA exosome complex core is conserved from prokaryotes to archaea and eukaryotes (Fig. 1) (1). These structures feature a central channel that is formed by a ring of six RNase PH-domains that can fit a single-stranded RNA molecule (7,10). In bacteria, the functional analog of the RNA exosome is the Polynucleotide Phosphorylase (PNPase) that forms a ring from six protomers with alternating PH-1 and PH-2 domains and a cap containing S1 and KH RNA binding domains (Fig. 1A) (11,12). Similarly, archaeal exosomes form a ring (barrel) consisting of three Rrp41 and Rrp42 heterodimers containing PH-1 and PH-2 domains respectively, akin to bacterial PNPases (Fig. 1A-B) (13–15). Like bacterial PNPases, archaeal exosomes have a cap comprised of three copies of Rrp4 and/or Csl4 subunits with S1 and/or KH domains (13,16). Rrp4 and Csl4 subunits are interchangeable and can form the cap as homo- or heterotrimers in archaea (13,17). The nucleolytic activity of both the archaeal exosome and bacterial PNPases is achieved by multiple phosphorolytic active sites within the central channel (Fig. 1A-B) (12,15). Subunits of the exosome cap are not catalytically active and the cap-less archaeal exosome barrel is stable and phosphorolytic active *in vitro*, however RNA binding by cap subunits aids processivity (13,14,16).

Eukaryotic exosomes structures are more complex since they consist of nine distinct subunits. Analogous to archaeal exosomes, the eukaryotic barrel is composed of Rrp41-like (Exosc4-6) and Rrp42-like (Exosc7-9) subunits with PH-1 and PH-2 domains, arranged in alternating order to form a pseudo-hexameric ring (Fig. 1C) (7,10). The cap is formed from subunits Exosc1-3, which contain the RNA binding S1 and/or KH motifs (7,10). Despite the structural similarities the eukaryotic core is, unlike the archaeal core, not stable without the cap *in vitro* (10).

Functionally, eukaryotic exosomes also differ from their archaeal counterparts since they lack phosphorolytic activity. In eukaryotes, the residues conferring this activity are mutated and consequentially, the exosome core is catalytically inactive (1,10,18). Instead,

this function is passed on to different hydrolytic exo-/endoribonucleases, with distinct cellular localizations. These are the primarily nucleolar distributive Exosc10 (Rrp6), the processive Dis3 (Rrp44) that can be found in both the cytoplasm and nucleus in yeast, but is mostly nuclear in mammals and the cytoplasmic Dis3 homolog Dis3L that is only present in higher eukaryotes (18,19).

To gain insights into a possible mechanism of eukaryotic exosome assembly, copurification experiments were done. In yeast it was possible to copurify the Rrp41/Rrp42-like dimers Rrp41/Rrp45 (Exosc4/Exosc9), Rrp46/Rrp43 (Exosc5/Exosc8) and Mtr3/Rrp42 (Exosc6/Exosc7) (10,14). However, this could only be partially recapitulated with the human proteins. While Exosc4/Exosc9 (Rrp41/Rrp45; shades of green in Fig. 1C) and Exosc6/Exosc7 (Mtr3/Rrp42; shades of blue in Fig. 1C) dimers could be copurified, this was not possible for Exosc5/Exosc8 (Rrp46/Rrp43; shades of purple). Instead, Exosc8 was only copurified in complex with Exosc6/Exosc7 and Exosc5 could not be copurified under any conditions tested (10). Merely based on such interaction studies, an association of preformed dimers of barrel subunits, akin to the assembly of the archaeal exosome, has been proposed for the eukaryotic exosome. Furthermore, since eukaryotic exosomes are unstable *in vitro* without the cap, it has been proposed that the cap subunits may stabilize the interactions between adjacent dimers by bridging them (10). However, systematic approaches that directly address the cellular assembly of eukaryotic exosomes are currently missing.

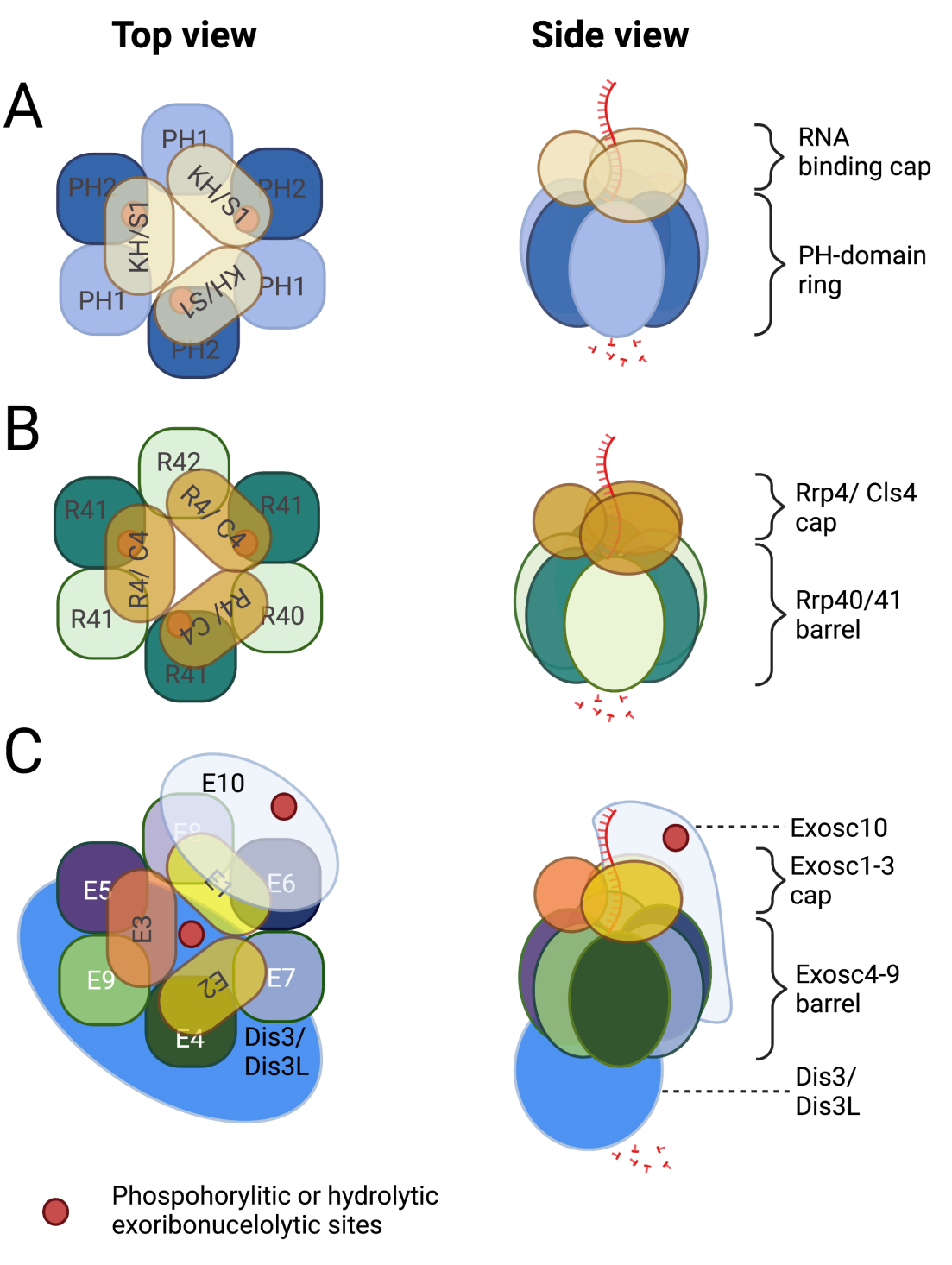

Figure 1: Molecular architecture of the major 3´-to-5´ exoribonucleolytic machineries in bacteria, archaea and eukaryotes. (**A**) Structure of bacterial PNPase. (**B**) Structure of archaeal RNA exosomes. C4 represents Csl4 and R**x** stands for Rrp**x**. The cap is not required for complex stability. (**C**) Structure of eukaryotic RNA exosomes with associated nucleases. E**x** represents Exosc**x**. Rrp40-like subunits Exosc7-9 are shown in lighter shades, Rrp41-like subunits Exosc4-6 are shown in darker shades. Models are based on structural data (10,12,13,20,21). Illustrations were inspired by a review of the eukaryotic exosome (1).

3.2 Different nucleases confer catalytic activity to the eukaryotic RNA exosome

Dis3 and its orthologues are part of the RNase II/RNR superfamily and are present in most organisms across all kingdoms of life (22). There is considerable sequence and functional conservation between yeast and human Dis3, as highlighted by complementation of mutant yeast Dis3 cells with human Dis3 (5,23). Dis3 in yeast is present in both the cytoplasm and the nucleus, while Dis3 in humans is mostly nuclear. Cytoplasmic exosome function of higher eukaryotes is mediated by the Dis3 homologue Dis3L (19). A third Dis3 homologue, Dis3L2, can also be found in higher eukaryotes, but functions in an exosome independent manner (24,25).

Differences between Dis3 homologues stem mostly from mutations in the PIN domain. This domain mediates the interaction with the exosome at the bottom of the barrel with Rrp41 (Exosc4) and Rrp45 (Exosc9) and is absent in Dis3L2 (19,20,25,26). Additionally, the PIN domain grants Dis3 a distributive endoribonucleolytic activity, that is absent in Dis3L and not essential for viability in yeast (19,27,28). Both the exo- and endoribonuclease activities of Dis3 are modulated by the exosome core, but are present without it *in vitro* (29). RNA is threaded as a single strand from top to bottom to the highly active hydrolytic site of Dis3 (20).

Exosc10 (Rrp6) is related to the bacterial RNase D and is a distributive, hydrolytic exoribonuclease (1). It is found in the nucleus being enriched specifically in the nucleolus, either bound to the exosome core alone or together with Dis3 (1,19). Association with the exosome is achieved via interactions with the cap subunit Exosc1 and the barrel subunits Exosc6 and Exosc8 (20). Structural studies revealed that the exoribonuclease domain and active site of Exosc10 are solvent-exposed (30). This potentially explains the distributive activity as there is no channel present that could bind or guide RNA to the active site (1).

Binding of Exosc10 enhances Dis3 activity, while binding of (catalytically inactive) Dis3 strongly reduces Exosc10 activity (29). Exosc10 is about 10-times more abundant than Dis3 in human cells (19), but is not required for cell survival in yeast (4). Nuclear exosomes associated with both Dis3 and Exosc10 exist, but exosome cores associating with Exosc10 alone can also be found, primarily in the nucleolus (19). Many substrates of Exosc10 are proposed to be core-dependent, but some substrates may be targeted in an exosome independent manner (31).

3.3 Substrate spectrum and specificity of the eukaryotic RNA exosome

Provided a single stranded 3′ terminus, Dis3/Dis3L can efficiently engage and degrade structured RNAs (10). For this purpose, the 3′ end is threaded through the barrel to the active site, a distance spanning 31-33 nucleotides (32). Thus, Dis3 dependent exosome functions rely on RNA-helicases that are part of adapter complexes, mediating exosomal degradation or processing of RNAs by conferring target specificity to the exosome complex (33). Both the path of RNA to Exosc10 and the interplay with some nuclear exosome adapter complexes remain subject of debate (34). Interestingly, the nuclear exosome associated RNA helicase Mtr4 binds to the top of the exosome seemingly displacing the catalytic domain of Exosc10 from the cap, suggesting mutual exclusivity between the two (35–37).

In the nucleus, the substrate-bound helicase Mtr4 is recruited to the exosome core as part of the nuclear exosome targeting complex (NEXT), the poly(A)-tail exosome targeting complex (PAXT) and the Trf4/Air2/Mtr4p polyadenylation complex (TRAMP) (38,39). NEXT associated exosomes are implicated in the degradation of introns from pre-mRNAs and pervasive transcripts like promoter upstream transcripts (PROMPTs) or enhancer RNAs (eRNAs). Additionally, snRNAs, snoRNAs, long terminal repeats and telomerase RNAs that are aberrantly 3′ extended are degraded in dependence on NEXT (33,38,40–43).

PAXT channels RNAs with longer poly(A)-tails, such as some PROMPTs, lncRNAs, eRNAs and prematurely terminated transcripts to the exosome (39,44).

TRAMP contains a poly(A) RNA-polymerase that adds an oligo(A)-tail to the 3′ ends of RNAs, stimulating exosomal decay or processing of aberrant tRNAs, pre-rRNAs and mature rRNAs, several snRNAs and snoRNAs, as well as certain ncRNAs like cryptic unstable transcripts (CUTs). TRAMP-dependent poly(A)-tailing mediated degradation also targets abortive Pol I transcripts as well as centromeric RNAs and heterochromatic RNA as part of co-transcriptional gene silencing (45–52).

Additionally, the nuclear exosome processes some precursor miRNAs and plays a role in resolving transient DNA-RNA hybrid structures termed R-loops by degrading the nascent RNA (48,53,54).

In the cytoplasm Dis3L is responsible for exosomal exoribonuclease activity (19,55). While bulk turnover of mRNA in the cytoplasm is performed 5′ to 3′ by Xrn1, the contribution of 3′ to 5′ decay varies between organisms and is subject of debate (56–58). The cytoplasmic exosome plays a more specialized a role in cytoplasmic mRNA decay, particularly in turnover of histone mRNAs, short-lived A/U-rich elements (ARE), such as growth factor and cytokine transcripts (6,48,58,59). Additionally, ribosome-associated quality control is performed by the cytoplasmic exosome in the form of nonsense mediated decay, no-go decay, and non-stop decay mediated by the Ski-complex, containing the helicase Skiv2l (56,57,60–63).

Due to the wide array and significance of exosome-mediated functions, few exosome-associated diseases are known, as most mutations are not compatible with cellular viability. Typically, these mutations are missense mutations and often have tissue specific phenotypes (6). Symptoms associated with those mutations are manifold and include premature aging, loss of hearing and vision, intellectual disabilities and several different neurodegenerative diseases, particularly pontocerebellar hypoplasia type 1b and 1c (6,64–67). Additionally, Dis3 mutations are implicated in a number of cancers, particularly multiple myeloma, colorectal carcinomas, chronic lymphocytic leukemia and acute myeloid leukemia (28,68–71).

Moreover, the exosome plays a role in development and differentiation to certain cell types, likely because this requires post-transcriptional regulation to complement transcriptional reprogramming (72). In most cases, downregulation of the exosome favors differentiation over proliferation of progenitor cells (72). Involvement of the exosome in progenitor proliferation, skin epidermal and erythrocyte differentiation as well as B-lymphocyte maturation have been described (35,53,72–75).

In conclusion, the exosome is a central factor in the lifecycle of many different classes of RNAs, thereby regulating numerous cellular and system biology processes.

3.4 Genetic perturbation by inducible Cas9 system

To investigate the role of gene products in a physiological context, genetic perturbation can be used. One such strategy employs a bacterial and archaeal system using clustered regularly short palindromic repeats (CRISPR) and CRISPR associated gene products (Cas). CRISPRs were first described in *Escherichia coli* (76) and later found as well in archaea (76,77). CRISPR clusters consist of repeats that are separated by spacer sequences. Spacer sequences are of extrachromosomal and viral origin, however cells harboring homologous spacer sequences are not infected by corresponding viruses (78–80). In fact, CRISPR serves as a flexible and instructible defense system against foreign genetic elements (81).

Different classes of CRISPR effector proteins exist, the best studied and most used one being the endonuclease Cas9, which cleaves target DNA (82,83). Target specificity and recognition is conferred to Cas9 by the crRNA's spacer sequence, which hybridizes with a complementary target (protospacer), leading to the sequence specific cleavage of the target (84,85). Additionally, the presence of a short sequence protospacer adjacent motif (PAM) is required for target cleavage (78,86). An RNA with partial complementarity to crRNA, called tracrRNA, is required for crRNA maturation and activity (87). Full maturation and Cas9 activity can be achieved by expressing crRNA and tracrRNA as a single molecule, called single guide RNA (sgRNA) (87,88).

CRISPR-Cas9 based strategies can be used to generate highly specific genetic knockouts (KOs) of almost any gene. Endonucleolytic cleavage by Cas9 introduces a DNA double-strand break that is repaired by error-prone non-homologous end joining leading to deletions or insertions (indels) of a few nucleotides at the editing site (89). Indels can cause frame-shift mutations, changing the subsequent amino acid sequence and introducing premature stop codons, leading to the expression of a truncated and likely non-functional protein or non-sense mediated mRNA decay (90,91). However, by chance some double strand breaks will cause in-frame mutations, leading to the expression of potentially functional proteins. Thus, when generating KO cell lines using CRISPR-Cas9, the number of inserted or deleted nucleotides needs to be assessed to exclude clones harboring in-frame mutations. Generating such KO cell lines is limited in throughput and time intensive. Additionally, compensation of the lost gene may occur during clonal selection and essential genes are precluded from being studied this way (92,93).

To overcome these limitations, inducible KO systems have been developed. They allow for induction of Cas9 expression by addition of a chemical compound, like tetracycline (tet) in Tet-On or Tet-Off systems (94,95). In these systems, Cas9 expression is regulated by a promoter containing tetracycline responsive elements (TRE) and binding of tetracycline repressors (TetRs) to the promoter leads to repression of the promoter. However, fusion of the TetR protein with the virally derived VP16 transcription activator domain results in tet-controlled transcriptional activator (tTA) proteins that activate gene expression by binding to a promoter (96).

In Tet-Off systems, tTAs are removed from the TRE if bound to tetracycline class antibiotics like tetracycline or doxycycline, thereby turning transcription off (95,97). In this thesis, a Tet-On system was employed, based on a mutant TetR binding the promoter in presence of doxycycline (Fig. 2) (94). Due to the reversed activity of the TetR, the respective VP16 fusion proteins are called reverse tet-controlled transcriptional activator (rtTA) (97).

Since Cas9 mediated mutations occurs randomly in each cell of the population, in-frame mutation harboring cells are an issue when analyzing phenotypes on a heterogenous population basis. To overcome this problem dual sgRNA systems have been developed, that allow simultaneous targeting of two regions of one gene (98,99). Thereby, the chance of introducing at least one frameshift mutation is increased substantially. Additionally, if Cas9 editing occurs at both sgRNA target sites in short succession, the sequence between the target sites may be cut out entirely. To further enhance the probability of successful disruption of protein function, sgRNA target sites can be improved. For example, the VBC score predicts optimized sgRNA sequences based on the conservation of different regions of the protein of interest and other parameters (100).

In this thesis, a Tet-On system for Cas9 expression was used in combination with a dual sgRNA strategy where sgRNA design was based on the VBC score. Protein levels and therefore the molecular impacts of depletion are dependent on knockout efficiency, cell-cycle time, and protein stability.

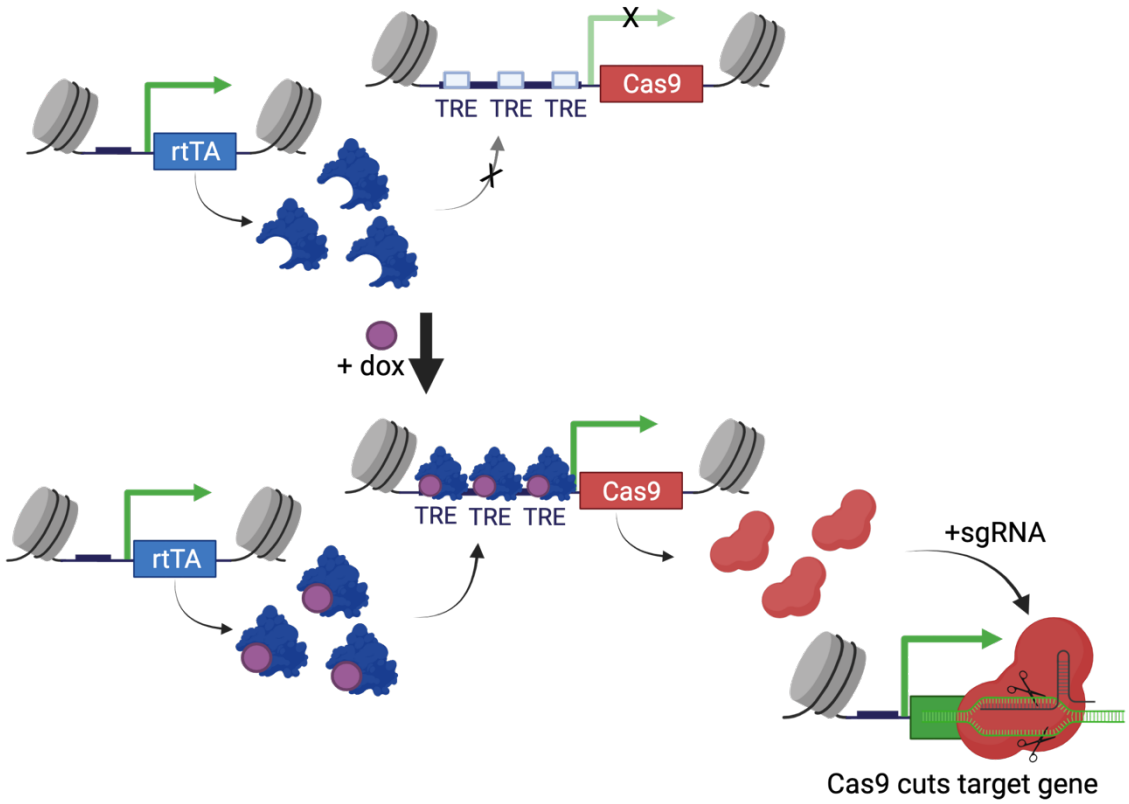

Figure 2: Genetic perturbation by an inducible Cas9 system. Schematic depiction of the Tet-On system. Addition of doxycycline (dox) leads to binding of rtTA to TRE of the inducible promoter and transcriptional activation. Consequential expression of Cas9 leads to sgRNA dependent cleavage of a target gene.

4 Aims of this thesis

With the work presented here, I aimed to establish an inducible Cas9 system in mESCs using a dual sgRNA targeting strategy for the efficient and reliable depletion of essential and non-essential gene products in a time-resolved and high throughput-compatible manner. I aimed to evaluate depletion efficiency and temporal-resolution of the system and put them in perspective to secondary effects like cell proliferation defects. I aimed to thereby define a window of opportunity of high protein depletion and low secondary effects which could be used to study direct molecular consequences of protein depletion.

The RNA exosome core consists of nine subunits and serves as a scaffold for a multitude of different RNA processing and degradation processes. Exosome-mediated functions have been studied in the context of the whole complex, but knowledge about contributions of individual subunits is limited. In this thesis, I strived to address such individual contributions by systematically depleting RNA exosome subunits with the previously mentioned inducible KO system and evaluating the corresponding phenotypes. Specifically, I aimed to investigate to what extend individual RNA exosome core subunits are required to achieve degradation of major RNA exosome substrates and maintain essential functions necessary for viability of mESCs.

Successful assembly of the RNA exosome *in vitro* enabled the resolution of the complex structure more than 15 years ago. However, the *in vivo* complex assembly process has not been conclusively resolved, mostly due to technical limitations. I set out to use the dual sgRNAs inducible Cas9 system with the goal to investigate co-destabilizations of exosome core subunits upon depletion of other exosome core subunits to uncover the cellular hierarchies in RNA exosome assembly.

5 Results

5.1 Efficient genetic perturbation with an inducible Cas9 system

A Tet-On system for inducible Cas9 expression in mouse embryonic stem cells (mESCs) was used to determine the individual roles of exosome core subunits for exosome activity and complex assembly (Fig. 2). This system was previously established in the lab through random lentiviral integration of a construct expressing rtTA and hygromycin resistance from two separate promoters. After selection with hygromycin, a construct for TRE-promoter controlled Cas9 expression was introduced to a random genetic locus using l a lentiviral vector strategy. In this construct, Cas9 was translationally coupled through a self-cleaving P2A peptide with BFP. Clonal cell lines were established from single cells that showed BFP expression upon doxycycline treatment.

Besides the components of the inducible Cas9 system, cells also constitutively expressed eYFP-Tir1 and endogenously tagged AID-Xrn1. Initially, this was done to study the effects of depletion of different cytoplasmic RNA decay machineries but is irrelevant for this thesis. It was previously shown in our lab that presence of eYFP-Tir1 and AID-tagged Xrn1 does not affect RNA-Seq profiles or cell viability (Supplementary Fig. S1A-B). AID-tagging reduced Xrn1 protein levels by 15 %, which is not expected to influence any results presented here (Supplementary Fig. S1C).

First, optimal conditions for KO induction and penetrance of genetic perturbance had to be assessed. To this end, the optimal concentration of doxycycline for Cas9 expression was determined. Treatment should have no adverse effects on cellular fitness, while leading to sufficient Cas9 expression for high KO efficiency.

Thus, cells were treated with different concentrations of doxycycline for 24 h or 72 h and viability was assessed in a luciferase-based assay (Fig. 3A). Viability remained above 95 % when using 100 ng/mL and 500 ng/mL while dropping to approximately 90 % when treated with 1000 ng/mL. Treatment for 72 h was slightly more detrimental than 24 h treatment.

To determine doxycycline concentrations needed for sufficient induction of Cas9 expression, a gene for a sgRNA targeting the chromocenter of eYFP and a puromycin resistance gene were introduced to the cells through random lentiviral genomic integration (Supplementary Fig. S1D). Following puromycin selection, cells were incubated with varying doxycycline concentrations and remaining eYFP signal was measured after 24 h and 48 h (Fig. 3B).

As expected, higher doxycycline concentrations led to faster depletion of eYFP signal, especially after 24 h of treatment. However, depletion efficiency was almost identical at 94 % - 98 % after 48 h for concentrations between 500 ng/mL to 1000 ng/mL doxycycline (Fig. 3B). This suggests that Cas9 expression is induced faster at higher concentrations of doxycycline, but ultimately concentrations of 500 – 1000 ng/mL doxycycline are sufficient to mediate KOs with maximum achievable penetrance and speed. Considering this and the viability data (Fig. 3A), 500 ng/mL doxycycline was selected as the optimal concentration for Cas9 induction and used in all further experiments. Leaky Cas9 expression in absence of doxycycline would prohibit precise temporal control of KO induction, however anti-eYFP sgRNAs expressing cells were not treated with doxycycline and did not exhibit a decrease in eYFP signal (Fig. 3B), suggesting that Cas9 expression is tightly

controlled. The efficiency of this anti-eYFP sgRNA had been established in the lab before, but KO efficiency of the inducible Cas9 system targeting other genes might be limited by poor sgRNA targeting efficiency and in-frame indels following Cas9 mediated endonucleolytic target cleavage. To overcome these limitations, a dual sgRNA system was employed as described previously (101). Using two different sgRNAs to target the same gene decreases the chances of poor targeting efficiency and in-frame mutations and can lead to the removal of the sequence between the sgRNA targeted site. Additionally, sgRNAs were designed according to the VBC score, that considers amongst other things, the conservation of different regions of the target gene (100). Thus, even an in-frame indel at a highly conserved region is unlikely to be expressed as a functional protein, increasing the probability of generating functional KOs with high penetrance in the population. A lentiviral construct for expression of dual sgRNAs and puromycin resistance from separate promoters was randomly integrated to the genome prior to Cas9 induction with doxycycline and cells were subjected to puromycin selection.

Exosc3 was depleted to 25 % after 24 h of induction and 5 % protein remained after 72 h (Fig. 3C-D). Treatment for 96 h did not increase the depletion efficiency, likely due to the high selective advantage of cells with stochastically slower or weaker Cas9 induction or Cas9 silencing. Keeping the cells for more than 96 h after KO induction was not possible due to cell death. In contrast, no reduction in Exosc3 abundance was observed in untreated cells after 96 h, arguing for tight control of Cas9 expression. Exosc4 depletion followed a similar pattern with the highest degree of depletion observed after 72 h (Fig. 3E-F). However, the absolute degree of depletion was lower with 13 % of protein remaining in Exosc4 KOs compared to 5 % in Exosc3 KOs.

Besides efficient depletion of core subunits, Dis3L co-depletion was observed for both Exosc3 and Exosc4 KOs (Fig. 3C, 3E) which was previously reported upon siRNA-mediated knock-down of Exosc3 (19). Co-depletion occurred rapidly, as no Dis3L was detected after 24 h of Exosc3 depletion and only a weak band was observed in Exosc4 KOs after 24 h. At maximum depletion, Dis3L levels were reduced by at least 50 % in both cases, but antibody sensitivity and amount of loaded protein does not allow for more precise quantification as seen in the dilution series. Even so, the degree and speed of co-depletion is striking, considering that Dis3L expression is unperturbed. Thus, Dis3L protein half-life heavily depends on the presence of an intact exosome core.

In conclusion, exosome core subunits can be efficiently depleted with the inducible Cas9 system with the highest degree of depletion achieved after 72 h. How this relates to phenotypes like cell proliferation remained be determined, which was done next.

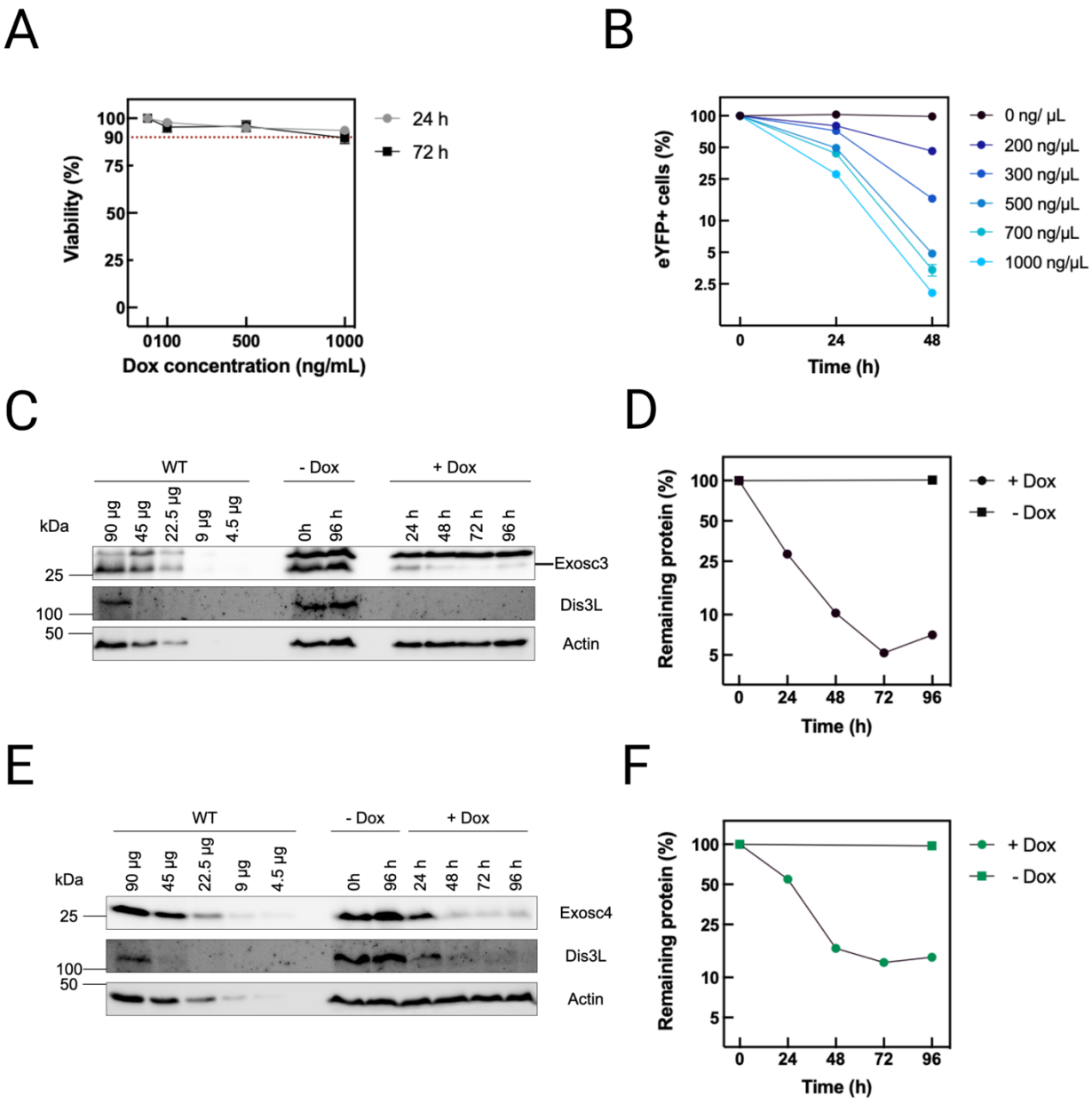

Figure 3: Efficient genetic perturbation with an inducible Cas9 system in mESCs. (**A**) Luciferase activity-based viability of cells treated with indicated concentrations of doxycycline (dox) for 24 h or 72 h. (**B**) Remaining eYFP+ cells expressing anti-eYFP sgRNAs after induction of Cas9 expression with indicated concentrations of doxycycline. (**C**) Western blots of Exosc3 KOs after different timepoints of Cas9 induction, probed with Exosc3 and Dis3L antibodies. Actin was used as a loading control. (**D**) Quantifications of Exosc3 signal from Western blot in D. (**E**) Western blots of Exosc4 KOs probed with Exosc4 and Dis3L antibodies. Actin was used as a loading control. (**F**) Quantifications of Exosc4 signal from Western blot in F.

5.2 Depletion of RNA exosome core components but not Exosc1 show severe proliferation defects in mESC

Results presented previously in this thesis, showed that exosome core subunits could be efficiently depleted using the dual sgRNA inducible Cas9 system (Fig. 3C-F). However, the corresponding effects on cell growth remained to be determined. To inspect the physiological consequences of core exosome component depletion, I performed growth competition assays. To this end, mESCs were transduced with lentiviruses to facilitate expression of mCherry coupled through a self-cleaving P2A site with a puromycin resistance gene and two sgRNAs targeting individual exosome components. Following puromycin selection, those cells ($mCherry^+$) were mixed with parental cells ($mCherry^-$) expressing no sgRNAs (Fig. 4A). Cas9 expression was induced by adding doxycycline and the effect of exosome component depletion on cell proliferation over time was interrogated by measuring the ratio of $mCherry^+$ to $mCherry^-$ cells by flow cytometry.

To control for detrimental effects of Cas9 and sgRNA expression on cell growth, sgRNA-pairs against the non-expressed olfactory receptors Olfr10, Olfr23, and Olfr55 were used. Olfr10 and Olfr23 KOs showed no proliferation defects, however the fraction of Olfr55 KO cells dropped slightly but significantly over time, presumably due to off-target effects. In sum, these controls highlight that expression of Cas9 or sgRNAs alone did not lead to a drop in cell growth, but some growth defects may be caused by off-target editing. When similarly assaying induced knockouts of all core exosome components, I observed severe and comparable proliferation defects for most factors, except for Exosc1 and Exosc5 (Fig. 4C). Note that the fraction of Exosc5 KO cells dropped below 10 % after 168 h, indicating that KO penetrance was above 90 % and Exosc5 depletion is detrimental for cell proliferation. Thus, this delayed phenotype may be due to higher Exosc5 protein stability. On the other hand, Exosc1 KO cell fractions remained above 50 % after seven days of depletion. This is unlikely due to higher protein stability since the half-life of Exosc1 was reported to be the lowest of all the core exosome subunits (102). Such a growth phenotype could be due to low KO efficiency caused by insufficient target engagement by sgRNAs or due to a persistent activity of Exosc1 devoid exosomes. Generally, KO penetrance was high given that the relative contribution of the $mCherry^+$ population in most exosome core component depletions was below 5 %.

Similar growth competition experiments were performed for the exosome associated catalytic subunits Dis3, Dis3L and Exosc10 (Fig. 4D). KOs of exosome associated nucleases showed distinct differences in proliferation between the nuclear subunits Exosc10 and Dis3 and the cytoplasmic Dis3L. Dis3L is responsible for cytoplasmic exosome activity, which is not essential in mESCs, which is in line with the observed milder proliferation phenotype (58). Dis3 is expected to be essential in mammalian cells, like it is in yeast, explaining the steeper drop in viability of Dis3 compared to Dis3L depleted cells (18,28). The impact of Exosc10 inducible KOs on cells is remarkable, considering its reported non-essentiality in yeast (2,3,5,6). However, it is not possible to draw direct conclusions from growth competitions to essentiality of a gene.

Depletion of all Ski-complex proteins, the cytoplasmic exosome adapter complex, showed similar effects on cell growth between themselves (Fig. 4E). Compared to depletions of core subunits (Fig. 4B), the proliferation defects were less pronounced, which is in line with the reported essentiality of exosome core factors and the non-essentiality of cytoplasmic exosome functions (2–6,56,58). Interestingly, Dis3L depletion had a less severe effect on cell viability than the Ski-complex components despite being involved in

the same pathway. The less severe proliferation defects of Dis3L compared to the Ski-complex might be due to low amounts of Dis3, which is mainly nuclear but can be found in the cytoplasm to small extends (19,28).

In summary, depletion of exosome core subunits and some associated factors mostly had the expected effects on cell proliferation. For instance, depletion of Ski-complex components and the cytoplasmic exoribonuclease Dis3L only showed moderate proliferation defects. Additionally, most core exosome components exhibited strong phenotypes, in line with their expected essentiality. Induced Exosc1 KO cells on the other hand showed far less severe proliferation defects, which is unlikely caused by higher protein stability. Instead, low KO penetrance or dispensability of Exosc1 for essential exosome functions could explain this observation.

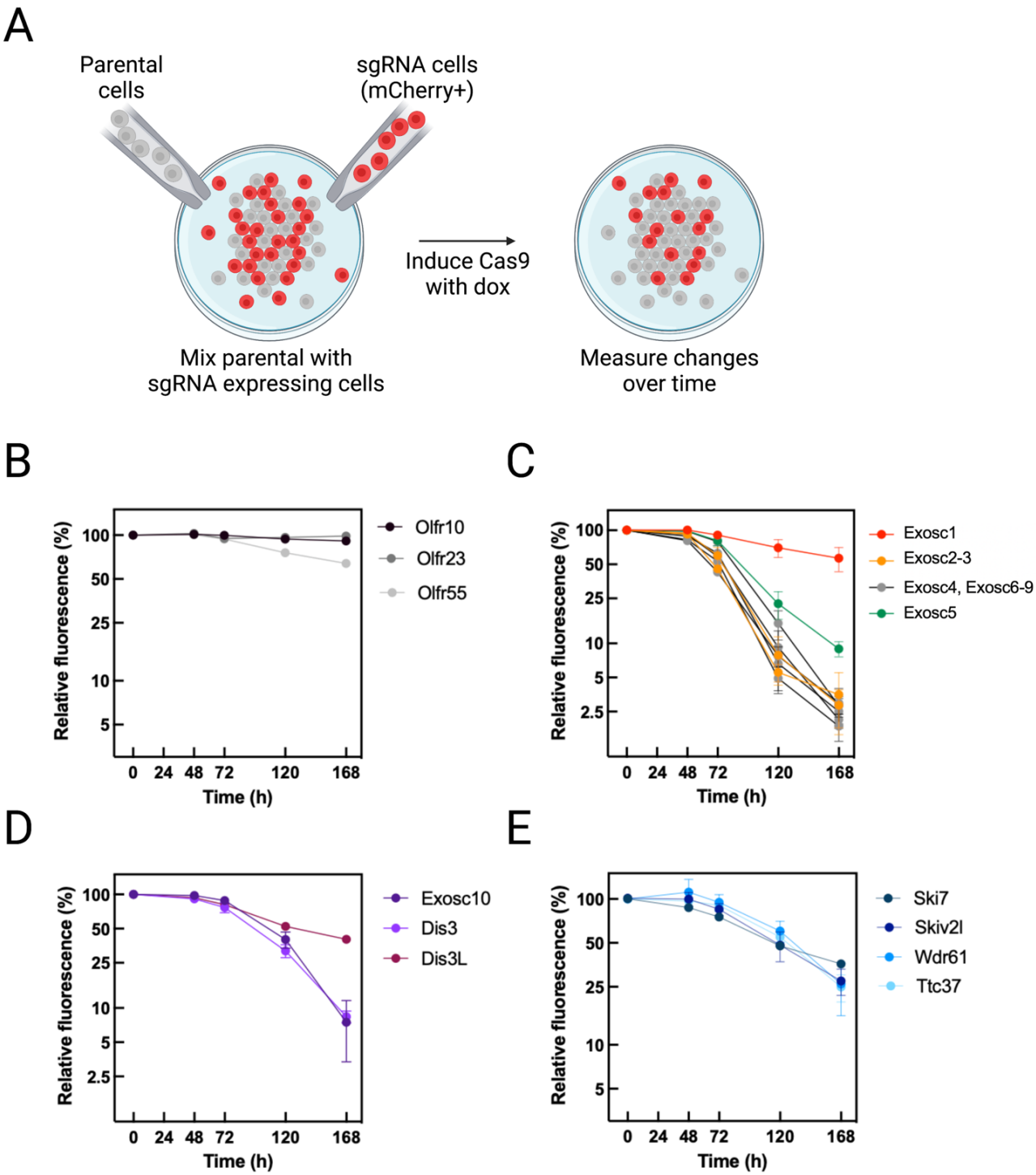

Figure 4: Growth competitions reveal Exosc1 as outlier amongst other core RNA exosome subunits. (**A**) Schematic depiction of the cell growth competition experiment set-up. (**B-E**) Growth competitions of indicated KOs versus the parental cell line. Error bars are SDs from biological triplicates, except Olfr55 which was not replicated. KOs of olfactory receptors served as controls since they are no expressed in our mESCs. In (C), exosome barrel subunits are shown in grey and cap subunits are shown in orange, with the exceptions of Exosc1 and Exosc5 respectively shown in red and green.

5.3 Exosc1 is partially dispensable for some exosome functions

Exosc1 stood out amongst the other exosome core subunits since the KOs showed a less severe growth phenotype (Fig. 4B), which could be due to poor sgRNA targeting efficiency. To address this, three additional pairs of sgRNAs were designed to target different regions of the protein (Fig. 5A) and KO efficiency of each was determined using Western blots (Fig. 5B). KO efficiency was above 90 % for all four sgRNAs pairs after 72 h of KO induction.

Notably, KOs with all four different sgRNAs performed similarly amongst each other in growth competitions and showed far less severe growth phenotypes than the median core subunit KO (Fig. 5C). Since the exosome's functions are indispensable for cell survival (4,6), these functions may be sufficiently upheld in Exosc1 KOs.

To investigate molecular phenotypes, an RNA-Seq dataset of Exosc1 inducible KO cells was generated in our lab and part of the analysis is presented in this thesis. This molecular characterization is aimed to detect direct effects of Exosc1 depletion. Thus, a window of opportunity was defined that combines low protein levels with low secondary effects. For this purpose, Exosc3 was depleted, and growth competition data was compared with Exosc3 protein levels as determined by Western blot (Fig. 5D). The window of opportunity was defined from 24 h to 72 h of KO induction with 28 % and 5 % of protein remaining respectively and corresponding mCherry signal of 96 % after 24 h and 71 % after 72 h. For the purpose of RNA-seq, the 48 h KO induction timepoint was chosen since this timepoint offers high depletion levels combined This was done with all core exosome components as well as factors involved in cytoplasmic mRNA decay.

Data derived from RNA-Seq was plotted in a principal component analysis (PCA) (Fig. 5E), where most of the variability is explained by PC1. Core exosome components, shown in grey (barrel) and orange (cap), clustered away from other factors along the x-axis (PC1). Exosc5 is positioned closer to non-exosome factors than other core subunits, which is in line with the observations made in the growth competitions (Fig. 4C).

The only core subunit that clustered away distinctly from other core subunits was Exosc1 (Fig. 5E). In fact, it was positioned closer to cytoplasmic factors (Ski-complex, Dis3L) and the control (Olfr10). Interestingly, factors involved in 5′ to 3′ decay (Xrn1) and 3′ to 5′ decay (Dis3L, Ski-complex) could be distinguished along the y-axis (PC2).

Next, the ability of the nuclear exosome to degrade PROMPTs was assessed by binning and plotting reads from various PROMPTs (Fig. 5F). Again, a striking difference was observed between KOs of other core exosome subunits and Exosc1, indicating partial functionality of the nuclear exosome in the absence of Exosc1.

Surprisingly, KOs of nuclear catalytic subunits Exosc10 and Dis3 showed similar degrees of PROMPT upregulation as Exosc1, despite good depletion of both after 48 h (Supplementary Fig. S11, S12). Thus, the weak PROMPT upregulation might be due to partial functional redundancy between the two. Alternatively, the kinetic bottleneck of PROMPT degradation may be the channeling of the RNA to the catalytic site. In this case, low levels of enzyme might be able to maintain the decay functions better than low levels of core complex. To test this, PROMPT levels would have to be assessed at later timepoints as well.

Regardless, Exosc1 clearly stands out amongst the core exosome components regarding both molecular and proliferation phenotypes, despite efficient depletion (Fig. 5B-C, E-F). In fact, clonal cell lines of Exosc1 KOs were established in our lab, highlighting the long-term viability of Exosc1 devoid mESCs (data not shown). Together this suggests that some functions of the RNA exosome, particularly the ones required for cell viability, are at least partly maintained in the absence of Exosc1.

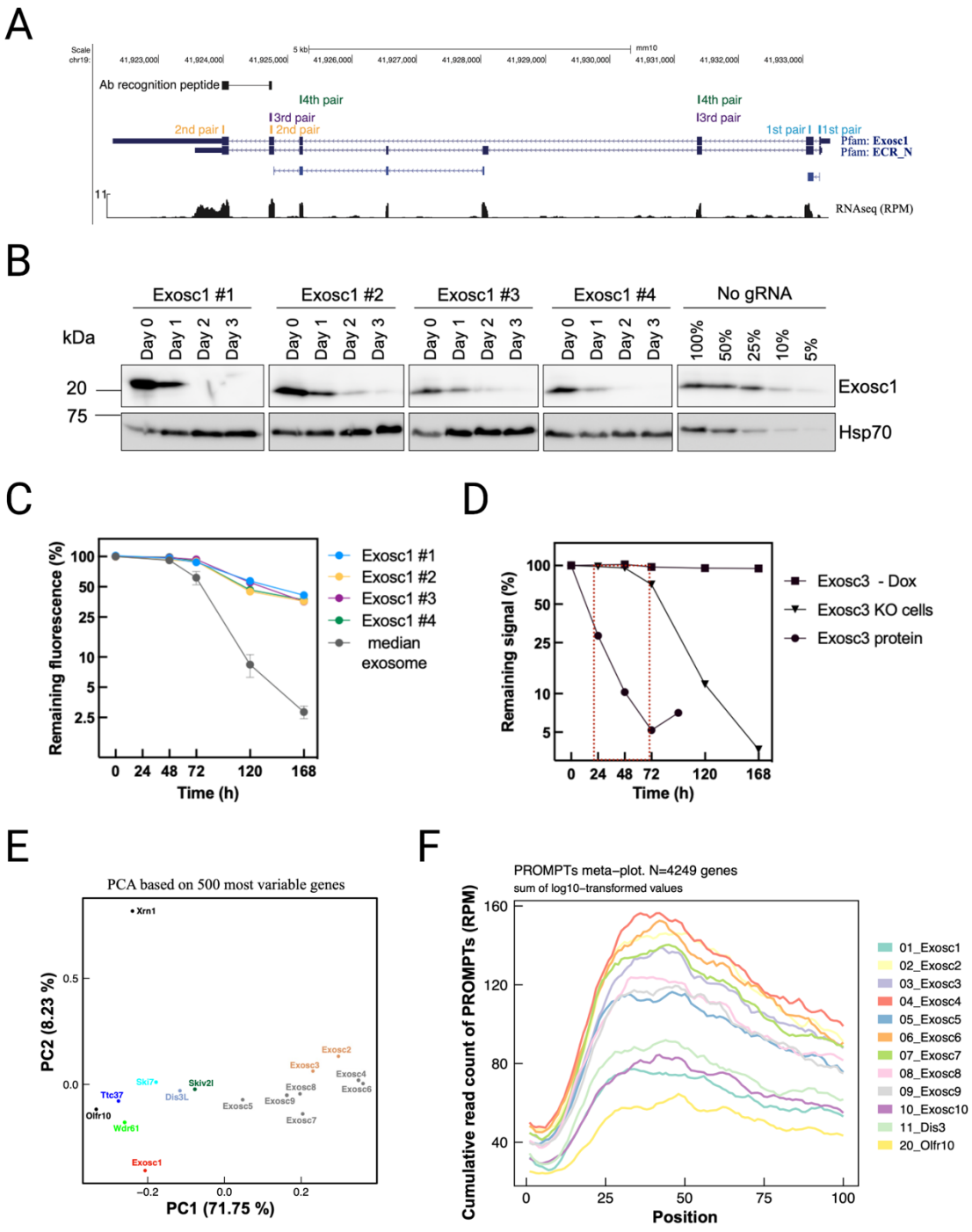

Figure 5: Exosc1 is partially dispensable for exosome function. (**A**) Overview of the Exosc1 gene and binding sites of the four different sgRNAs pairs. Additionally, the antibody (Ab) binding site is shown. (**B**) Western blots analyses confirming depletion of Exosc1 targeted by 4 different sgRNA pairs. Positions of sgRNA targets are indicated in (A). (**C**) Growth competition of median core exosome and Exosc1 KOs with different sgRNAs. Error bars are SD from technical replicates. (**D**) Comparison of Exosc3 protein levels and remaining KO cells in growth competition assays. Red lines define the window of opportunity with low protein levels and low proliferation defects. (**E**) PCA of RNA-Seq data from 48 h of knockout induction. Exosome cap component shown in orange, barrel subunits shown in grey. (**F**) PROMPT read coverage after 48 h of KO induction of exosome core factors, associated nuclear ribonucleases and Olfr10 as control. Reads are binned into 100 positions and shown are the sum of log10-transformed values. N= 4249 genes. One replicate of RNA-Seq data is presented here.

5.4 RNA exosome core subunits assemble sequentially upon initial timer formation of Exosc2/4/7

Data from Exosc1 depletions and the viability of Exosc1 KO clonal cell lines made us reason that a functional exosome complex may exist in the absence of Exosc1, warranting further investigate into (sub-)complex formation in the absence of other core factors. Exosome core components Exosc2 and Exosc9 were shown to be unstable outside the complex due to proteasomal degradation in *Trypanosoma brucei* (103), hence we reasoned that any subunit replaced from the complex may be subject to degradation. Indeed, all exosome subunits were depleted if excluded from the assembling (sub-)complex. Therefore, if a subunit is required for a second subunit to bind the forming (sub-)complex, KO of the first subunit would lead to co-depletion of the second subunit.

Generally, unilateral or multilateral co-depletions would be possible. Unilateral dependency of one subunit on another indicates a sequential assembly mode where the knocked-out subunit is required upstream of the co-depleted factor in the assembly process. Mutual dependency of two or more subunits on the other hand indicates the formation of a dimer or multimer, that is only stable if all di- or multimerization partners are present. In fact, both unilateral and multilateral dependencies were observed, indicating different modes of interactions in the assembly process.

To examine these co-depletions, we used the inducible Cas9 system described before (Fig. 2) to separately deplete all exosome core subunits (Exosc1-9) as well as the associated nucleases (Dis3, Dis3L and Exosc10). Western blotting was used to assess protein levels after 24 h, 48 h and 72 h of depletion in biological replicates (Supplementary Fig. S2-S13). Protein levels were consistently lowest after 72 h of KO induction.

Therefore, samples from this timepoint were run to illustrate all co-depletions at once (Fig. 6A). In addition, Western blots from the time courses were interrogated to quantitatively describe co-dependencies (Fig. 6B). However, quantifications of Western blots rely on the assumption that a linear relationship between protein levels and signal intensity exists, which is not always true (104).

To define the linear range for any blot, dilution series were prepared. Linearity depended heavily on the antibodies used and amount of protein loaded. In fact, in some cases near perfect linearity was observed between all timepoints (Fig. 6C). However, deviations from linear behavior were also observed, illustrated by a disproportionally strong signal in low range of protein abundance or too weak signal high protein abundance range (Supplementary Fig. S14). Both are common issues and could sometimes be observed on the same blot (Fig. 6D). These issues were described previously as Western blot intrinsic limitations (104) and are unlikely due to poor quality of the dilution series itself since both perfect linearity and poor linearity could be observed on images from the same blot (Fig. 6C-D). Both linear range and detection limit were considered when quantifying the Western blots (Materials and Methods) to generate a heatmap of averaged values after 72 h of KO induction (Fig. 6B).

All exosome core subunits were depleted to less than 15 % and reproducible co-depletion patterns were observed (Supplementary Fig. S2-S13). Depletion of Exosc2, Exosc4 and Exosc7 led to the co-depletion of all other factors except Dis3, which was only depleted in Dis3 KOs (Fig. 6A-B). Therefore, we concluded that Exosc2/4/7 form a heterotrimer that requires presence of all three subunits to be stable. This is in line with structural data,

according to which Exosc2/4/7 share a large interaction surfaces (Fig. 6E) (10). The strong dependency of other core subunits on those three subunits indicates that trimer formation is the first step in exosome core assembly.

Next, Exosc6 depletion led to co-depletion of all core subunits except the Exosc2/4/7 heterotrimer and must therefore be assembled upstream of all co-depleted factors. Similarly, all remaining subunits were dependent on Exosc8, indicating that binding of Exosc8 is the next step in the assembly. This order of events is in line with the reported structure of the complex, considering that Exosc6 interacts with Exosc7 and Exosc8, but Exosc8 does not interact directly with either trimer subunit (Fig. 6E) (10). Thus, Exosc6 binds to the Exosc2/4/7 trimer followed by Exosc8 binding to Exosc6.

Thereafter, Exosc9 can stably associate likely by binding Exosc4, which is required for the binding of all remaining factors. Alternatively, Exosc9 may to some extend associate with Exosc4 before Exosc6/8 recruitment. Exosc9 was depleted to a lesser extend in Exosc6/8 KOs (30-40 %), compared to high co-depletion in Exosc2/4/7 KOs (<10 %) (Fig. 6B). Therefore, Exosc9 binding of the trimer may be possible in the absence of Exosc6/8, which do not interact directly with Exosc9. However, there is likely a conformational change that makes the interaction of Exosc9 with the Exosc6/8 bound subcomplex more stable than the interaction with the Exosc2/4/7 trimer.

Exosc9 strongly interacts with Exosc5 in the assembled complex (Fig. 6E) (10) and Exosc9 binding precedes recruitment of Exosc5 to the subcomplex. Thus, the barrel is completely assembled with only one cap subunit (Exosc2). Following this, Exosc3 may bind the top of Exosc5 and Exosc9. Exosc1 protein levels depend on all other core subunits (Fig. 6A-B), and it is therefore the last component in the assembly of the exosome core. However, Dis3L seems to bind the complex already in the absence of Exosc1 since depletion of Exosc1, unlike the other core subunits, does not affect Dis3L levels.

On the other hand, at which stage of complex formation Dis3 interactions are stable could not be resolved since Dis3 is never co-depleted in KOs of any core subunits. However, interaction of Dis3 with the exosome depends on its PIN domain that is largely conserved to Dis3L (19,20). Thus, it is likely that Dis3 and Dis3L exosome binding are possible at the same stage of complex formation. This suggests that Dis3 can associate with Exosc1 deficient exosomes, which is in line with the previously discussed maintenance of exosome functions in Exosc1 deficient exosomes.

While seemingly dispensable for Dis3L and presumably for Dis3 binding, Exosc1 is required for Exosc10 stability (Fig. 6A-B). Again, this is in line with structural studies showing direct interactions of Exosc10 and Exosc1 (Fig. 6E) (20). The strong dependency of Exosc10 stability on all core subunits was unexpected, considering that Exosc10 was assumed to have core independent functions (31). However, whether the residual Exosc10 in Exosc1 depleted cells, is loosely associated with the core, functions independently from it or neither cannot be concluded from the data presented here.

Beside co-depletions, apparent stabilizations of other factors in the KOs were observed but are unlikely to be true biological effects and rather technical noise. Generally, stabilizations were rare and log2 fold changes were less than 0.35. Additionally, they could usually not be reproduced between the replicates. Contrary to depletions, apparent

stabilizations were not consistent or increasing throughout different timepoints, indicating that they are not true effects.

In summary, reproducible strong co-depletions of exosome core subunits enabled the resolution of the exosome complex assembly. In short, a heterotrimer of Exosc2, Exosc4 and Exosc7 is formed, followed by individual addition of Exosc6, Exosc8, Exosc9 and Exosc5 in that order. Therefore, the barrel is formed with Exosc2 being the only cap subunit. Subsequently, Exosc3 followed by Exosc1 binding completes the assembly of the core exosome. However, Exosc1 seems not to be required for Dis3L and by extension likely Dis3 association. Thus, the assembly model complements previous described phenotypes of Exosc1 KOs (Fig. 5) from a complex formation and stability standpoint. However, Exosc1 seems to be required for efficient Exosc10 recruitment to the core exosome as the stability of the latter is strongly dependent on the former.

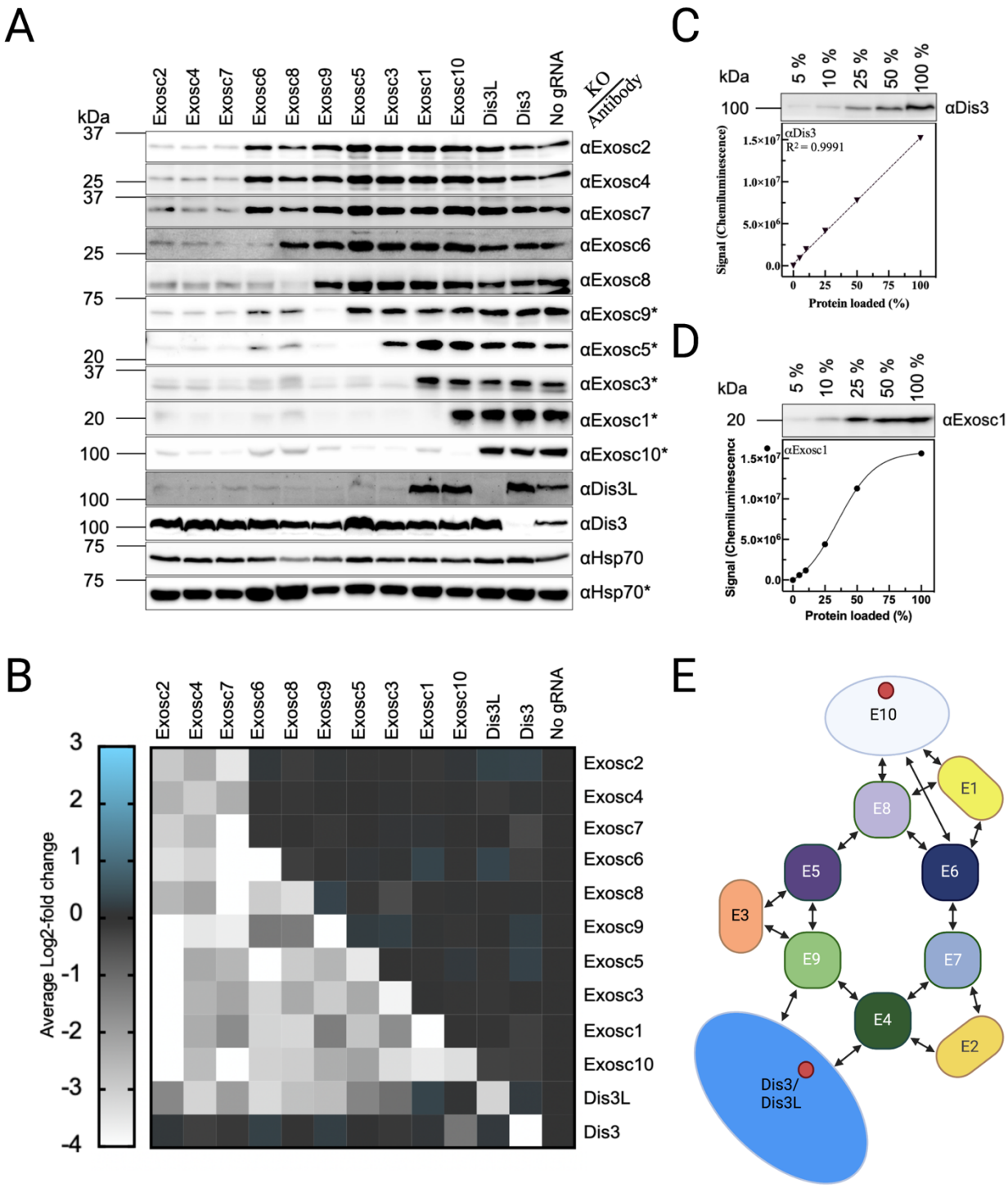

Figure 6: Subunits are recruited sequentially to the forming complex following initial trimerization of Exosc2/4/7. (**A**) Western blots illustrating co-depletions of subunits in specific KOs. Columns correspond to the KOs; rows indicate the antibody used to probe the respective subunit. Images were derived from two membranes. Asterisks indicate which Hsp70 is the corresponding loading control. (**B**) Quantifications of co-depletions from biological replicates of induced KOs after 72 h. (**C**) Dilution series used to determine linear range of signal from Dis3 antibody. (**D**) Dilution series used to determine linear range of signal from Exosc1 antibody. Both Exosc1 and Dis3 antibodies were used on the same blot, illustrating differences in linear range between antibodies. (**E**) Illustration of exosome subunit interaction map based on (10,19,20). E**x** stands for Exosc**x**. Large, shared interaction surfaces are indicated by arrows.

6 Discussion

6.1 An inducible dual-guide CRISPR/Cas9 system enables to experimentally address essential protein functions in mESC

When using a Tet-On inducible Cas9 system (Fig. 2), both the maximum achievable depletion efficiency and the stringency of Cas9 repression need to be evaluated to use the system most efficiently (95). Protein depletion efficiency is dependent on protein half-life, sgRNAs, KO penetrance and time after Cas9 induction and ideal depletion times are protein dependent. All exosome components could be depleted efficiently at the protein level, with highest depletion levels generally reached after 72 h of Cas9 induction (Fig. 3C-F, Fig. 6A-B, Supplementary Fig. S2-13).

Core components were depleted to at least 85 % after 72 h and, in many cases, protein levels fell below the detection limit of the antibodies. Even KOs of subunits like Exosc4 where protein depletion was less efficient (Fig. 3E-F), maintained a normalized population of less than 5 % in growth competition experiments after 168 h (Fig. 4F), indicating that KO penetrance was consistently higher than 95 %.

The limiting factor for KO penetrance is likely silencing of Cas9 or the rtTA, which were randomly integrated in the genome using lentiviruses. Hygromycin resistance was introduced together with rtTA and used to select for its integration. However, the hygromycin resistance gene was under the control of a different promoter than rtTA. Therefore, silencing of rtTA individually is possible. After multiple passages a reduction in Cas9 coupled BFP signal was observed, indicating reduction of Cas9 inducibility (data not shown). This could be due to Cas9 or rtTA silencing, which could be overcome by targeted integration to a ubiquitously active region like the Rosa26 locus (105).

The disparity between maximal protein depletion levels and KO penetrance derived from growth competitions, is likely due to the essentiality of the exosome core components. Cells in which Cas9 expression or Cas9 targeting of the genomic locus is less efficient, have a great selective advantage. Thus, these cells will outgrow or outlive cells that received the KO more efficiently but will ultimately be overgrown as well. Therefore, the population of cells induced to express Cas9 might be heterogenous regarding abundance of the targeted protein, depending on stochastic KO kinetics. This heterogeneity introduces noise when measuring effects of depletion, since the targeted gene will be expressed to different extents in different cells in the population.

Defining a window of opportunity to measure effects of protein depletion as directly as possible is important, to minimize secondary effects while protein depletion levels are high. This window of opportunity is more difficult to define in inducible KO systems than in for example an auxin inducible degron system that allows very rapid degradation of a factor and thus measurement of more direct effects of depletion. AID-systems are however more limited in throughput and may suffer from insufficient depletion and leaky degradation. In the case of exosome core subunits, the severe growth defects are not immediately following protein depletion. Thus, a window of opportunity could be broadly defined from 24 h to 72 h (Fig. 4B) of KO induction. Particularly the timepoints 48 h and 72 h showed high protein depletions with low to medium effects on cell growth, when depleting exosome core subunits.

One issue that must be considered when using CRISPR based strategies are off-target effects. While KOs of exosome core components were efficient, as confirmed by Western blot (Fig. 6A, Supplementary Fig. S2-13), off-target effects can never be excluded. They can be hardly controlled for individually, but one of our controls, Olfr55 KOs, showed reduced growth compared to parental cells (Fig. 4C). Since Olfr55 is not expressed in mESCs and KOs of Olfr10 and Olfr23 had no adverse effects on cell growth, this is presumably due to off-target action of Cas9. Increasing Cas9 expression might slightly increase KO speed (Fig. 3B) but might also increase off-target effects. Editing of the wrong genomic locus distorts growth competition data since effects of editing that locus will be measured as well.

This is unlikely to affect the readout of KOs of essential genes, like Exosc2-9 since the drop in cell fraction is already substantial in these. Off-target effects are unlikely to substantially alter their growth behavior since unspecific editing would have to perturb a gene that is highly essential and whose perturbation would have rapid effects.

Finally, promoter leakiness could introduce noise since KOs may already be facilitated if sgRNAs are expressed together with Cas9 before induction with doxycycline. This did not seem to be the case, given that both protein levels and the normalized fraction of cells in the growth competition remained stable in uninduced cells expressing sgRNAs (Fig. 3B-F, Fig. 4B).

Thus, the system shows high penetrance and depletion efficiency, and affords a window of opportunity to measure direct effects of protein depletion as well as a high stringency of Cas9 repression.

6.2 Exosc1 is the only non-essential core subunit in mammalian exosomes

Surprisingly, Exosc1 showed different molecular and growth phenotypes compared to other exosome core subunits (Fig. 5C-E), despite high knockout efficiency (Fig. 5B). In fact, Exosc1 is completely dispensable for survival of mESCs (data not shown).

These observations are complemented by the co-depletion data, showing Exosc1 binding requires an otherwise completely assembled complex and does not influence complex stability. Strikingly, co-depletions suggest that Dis3L and perhaps Dis3 can associate with the Exosc1 devoid core, making Exosc1 KOs stand out from KOs of other core subunits. Additionally, this observation offers a structural explanation for viability of Exosc1 KOs.

On the other hand, Exosc1 seems to be required for efficient recruitment of Exosc10 to the complex and thus, exosome mediated functions of Exosc10 may depend largely on the presence of Exosc1 (Fig. 6A-B). Besides interacting with Exosc1, Exosc10 also interacts with Exosc6 and Exosc8 and whether this is sufficient to recruit Exosc10 to the exosome remains unclear (20). If such a complex exists and would be catalytically active remains to be seen.

Considering that Exosc1 is dispensable for viability, Exosc10 dependent exosome functions might not be essential in mESCs like in yeast (3,5,23). Therefore, differences between Exosc10 KOs and Exosc1 KOs could elucidate the precise role of Exosc10 exosome independent functions that were proposed previously (31). One such difference was

observed in growth competitions, where Exosc1 KOs exhibited considerably less severe growth than Exosc10 KOs (Fig. 4E-F). Thus, exosome independent functions of Exosc10 may be maintained with the low levels of Exosc10 in Exosc1 KOs. It is possible that exosome independent functions of Exosc10 may be essential in mESC while the exosome dependent functions are not.

Exosome activity is heavily dependent on adapter complexes that associate with the cap (20,36). Whether this is possible in the absence of Exosc1 is formally not clear, but PROMPT levels (Fig. 5E) and viability of KO cells argue in favor of it. Whether the Ski-complex can associate with Exosc1 devoid exosome cap remains elusive.

Finally, it remains to be determined how conserved Exosc1 dispensability is. In fact, Exosc1 (Csl4) seems to be essential in yeast, but truncations of its RNA binding S1 domain and NTD are viable (4,29,106). This is in contrast to Exosc2 (Rrp4) and Exosc3 (Rrp40) whose S1 and KH RNA-binding domains as well as NTDs are indispensable for cell viability (106). Therefore, Exosc1 might not play an essential role in yeast exosome function, given that either domain the RNA binding domain is dispensable, but might still be required for complex stability. Exosc1 has been reported to play a lesser role in yeast complex stability compared to most other core subunits and its contribution to stability might have been further reduced during evolution to higher eukaryotes.

6.3 Resolving the cellular assembly of the RNA exosome

In archaeal exosomes Rrp41 and Rrp42-like heterodimers form the exosomal barrel, which is stable entirely without the cap (13,14,17). Copurification of yeast barrel subunits suggested that a similar assembly process might be conserved to eukaryotes (10,14). However, unlike its archaeal counterpart the exosomal barrel is not stable *in vitro* and copurifications done with yeast proteins could not be completely recapitulated with the human isoforms. Still, it was believed that the eukaryotic exosome assembly might be akin to archaeal assembly.

If exosome assembly required formation of barrel dimers, those dimers should be stable in the cell. Therefore, depletion of one dimer subunit should lead to the co-depletion of the dimerization partner and vice versa. Such a bilateral co-dependence was not observed for any subunit in our mESCs. The only multilateral dependency was observed between Exosc2, Exosc4 and Exosc7. Therefore, only unstable, if any, barrel heterodimers may exist in the cell. Those dimers would not be required for complex formation since stable subcomplexes can form with one presumed dimerization partner in the absence of the other. Thus, even if such unstable dimers exist *in vivo*, their presence would likely not have biological meaning. The fact that reported *in vitro* interactions are not relevant for complex assembly highlights the advantages of this co-depletion-based approach, since *in vivo* dependencies could be investigated.

The model proposed here (Fig. 7) is based on co-depletions of exosome factors in KOs of different subunits (Fig. 6A-B, Supplementary Fig. S2-13). It stands to reason that co-depletions are due to instability of subunits outside the complex which was reported before and shown to be due to proteasomal degradation in *Trypanosoma brucei* (103).

Instead of dimers joining together, the sequential addition of core subunits following initial heterotrimer formation is proposed (Fig. 7). In short, subunits Exosc2/4/7 form a

trimer that can then be bound by Exosc6, Exosc8, Exosc9 and Exosc5 in this order to complete barrel assembly. Finally, Exosc3 binding allows Exosc1 to associate and thereby complete complex assembly. This is to a certain extend reminiscent to the archaeal exosome assembly process, where the barrel can form entirely without any cap subunit (13,17).

Exosc9 seems to associate transiently with the Exosc2/4/7 trimer already, but the interaction becomes stable only after Exosc8 binding. The precise mechanism of this is not entirely clear, since Exosc8 and Exosc9 do not share large interaction surfaces in the assembled complex (Fig. 6E) (10). Thus, a conformational change of the subcomplex seems likely, enabling stable interaction of Exosc4 and Exosc9.

A stable exosome core can form in the absence of Exosc1 and Exosc3 (Fig. 6A-B), which is in agreement with thermal shift assays showing that Exosc1 and Exosc3 interactions with the core are less stable than other subunits (107). Dis3L might even be able to unstably bind the barrel in the absence of Exosc3 considering that Dis3L is co-depleted to 45 % in Exosc3 KOs and to an average of 20 % in other core subunit KOs (except Exosc1) (Fig. 6B).

Dis3L interacts with the exosome via a PIN domain that binds the bottom of the barrel between Exosc5 and Exosc9 (20). This interaction may therefore be possible following Exosc5 binding, which precedes Exosc3 association, but becomes fully stable only after Exosc3 is present. Thus, Exosc3 binding to the top of Exosc5/9 may stabilize a conformation that enables interaction with the PIN domain on the bottom of Exosc5/9. Interestingly, RNA protection assays suggest that the yeast exosome can bind Dis3 (Rrp44) in the absence of any cap subunit (Exosc1-3; Csl4, Rrp4, Rrp40) *in vitro* (108). This could be partially recapitulated with our *in vivo* mESC data, suggesting that Exosc1 and Exosc3 are dispensable for (partial) Dis3L binding. Only one cap subunit, Exosc2, is strictly required for Dis3L recruitment. Still, this yeast *in vitro* data supports the idea of Dis3 (Rrp44) binding to Exosc1/3 (Csl4/ Rrp40) devoid exosomes. This is unlikely to be functionally relevant in the case of Exosc3, given that Exosc3 KOs were comparable to KOs of other core subunits concerning growth competitions and PROMPT upregulation (Fig. 4F, Fig. 5D-E).

In this regard only Exosc1 KOs stood out as clear outliers as discussed before (Fig. 5 C-E). Co-depletions suggest that Exosc1 devoid exosomes can completely bind Dis3L and therefore likely also Dis3, providing a structural explanation for Exosc1 dispensability (Fig. 6A-B). While the viability of Exosc1 depleted cells was surprising, it was found previously that Exosc1 associates less tightly with the core than all other subunits (109). Despite this, Exosc1 seems to be required for efficient recruitment of Exosc10 to the complex and thus exosome mediated functions of Exosc10 may depend on presence of Exosc1. Exosc10 also associates with Exosc6 and Exosc8 (20) and whether their presence is sufficient to recruit Exosc10 to the exosome remains unclear.

Usually, exosome functions are studied by depleting individual core subunits. Since all core components were expected to be essential for complex function, any component might be chosen for complex disruption. However, Exosc1 deficient exosomes may remain partially functional, while depletion of Exosc2, Exosc4 or Exosc7 co-depleted all core subunits. Therefore, these three cores subunits seem to be the most suitable targets for depletion when studying the effects of exosome disruption.

How the exosome is imported to the nucleus where it performs most of its functions, is left to be determined. It is not clear whether the complex gets imported as a whole or is assembled in the nucleus. The lack of conserved nuclear localization sequences (NLS) in exosome core subunits suggests that assembly might take place in the cytoplasm and precedes nuclear import. In fact, it has been suggested that the NLS containing Dis3 (Rrp44) and/or Exosc10 (Rrp6) mediate import to the nucleus in yeast (110).

In that case, depletion of either Dis3 or Exosc10 could lead to a stabilization of Dis3L, since Dis3L stability seems to be highly dependent on (cytoplasmic) exosome levels (Fig. 6A-B). Dis3L abundance was increased by 5-15 % in Exosc10 and Dis3 KOs (Fig. 6B) which is not enough to confidently distinguish it from technical noise. Clearly, no strong stabilization takes place, but the maximum possible stabilization of Dis3L in the absence of nuclear import is unknown. Thus, no conclusions about nuclear import can be drawn from these observations and further investigations are required to resolve it as also discussed in the outlook section.

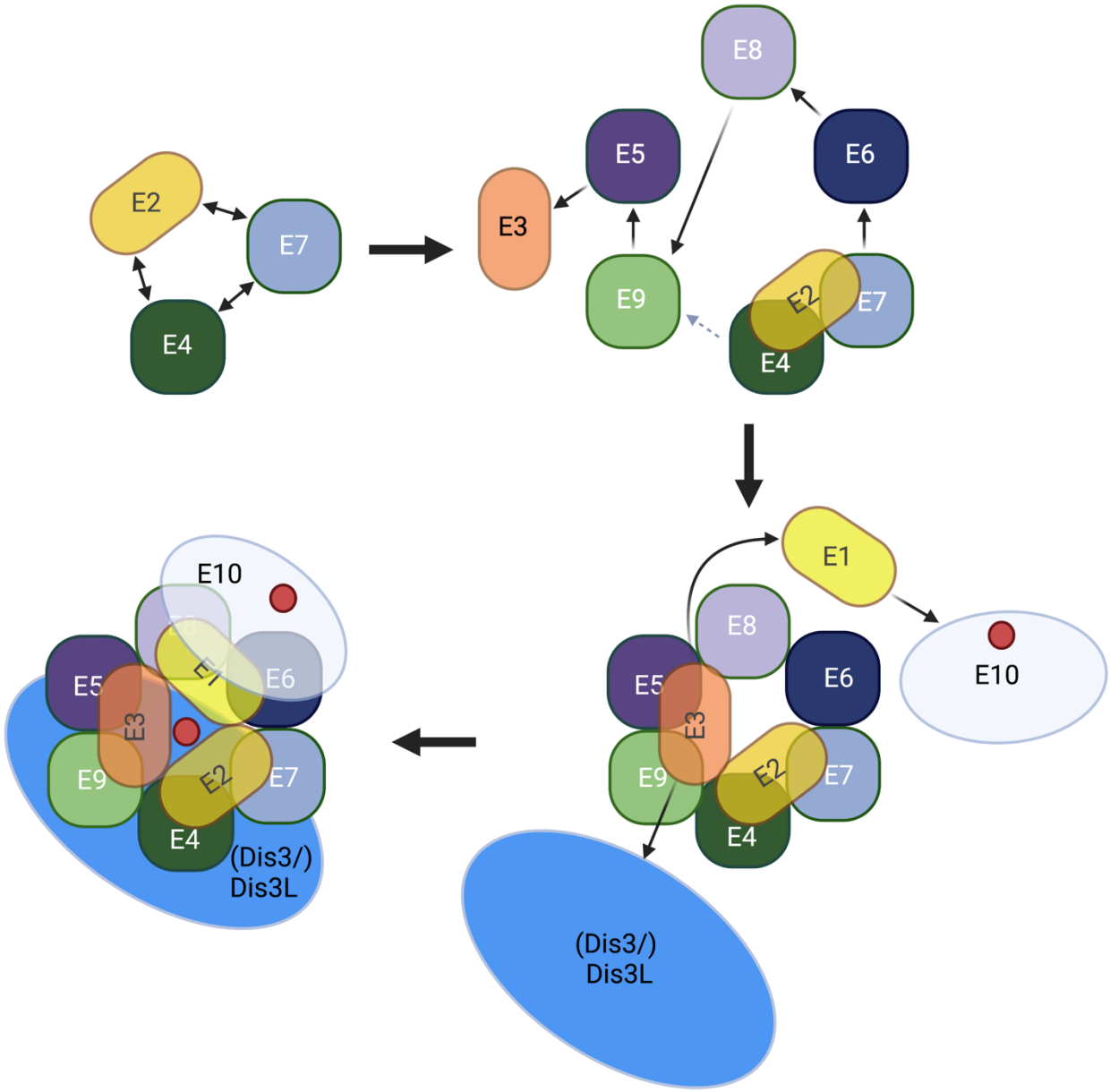

Figure 7: Cellular assembly model for the RNA exosome. The model is based on co-depletions shown in Fig. 6. Arrows indicate the order of assembly and two-sided arrows indicate co-dependence in the case of Exosc2/4/7 heterotrimer formation. The precise stage at which Dis3 can bind is likely the same as Dis3L, but conclusive evidence is missing. Not shown are unstable interactions of Dis3L with Exosc3 devoid exosomes. Exosc**x** are annotated as E**x**, with **x** being the number of the respective subunit.

6.4 Limitations of this thesis

As previously discussed, inducible Cas9 systems may be limited regarding protein depletion speed and KO penetrance. This limits the ability to measure direct molecular effects of protein depletion since it occurs gradually and depends on particular protein half-lives. Additionally, fast loss of cellular viability might influence the ability to measure other effects of the KO that take longer to come into play or have less severe phenotypes. However, observations made in this thesis are unlikely to be heavily influenced by this limitation. Particularly co-depletions to resolve exosome complex assembly should remain true regardless and were observed across three different timepoints (24 h, 48 h, 72 h).

Western blots are semi-quantitative and thus precision of quantification is limited by the linear range of the antibody detection. However, co-depletions were usually above 50 % and the complex assembly could therefore be modelled independently of precise quantification. In fact, the observation that Exosc9 might transiently bind to the Exosc2/4/7 trimer in the absence of Exosc6/8 and stably interacts only after integration of Exosc6/8 to the subcomplex speaks to the sensitivity of the method.

As discussed previously, formation of Rrp41/42-like dimers cannot be excluded formally but such dimers are unlikely to play a biologically relevant role in exosome assembly. Co-depletions observed here suggest a model of complex assembly independent of such dimers (Fig. 6A-B, Fig.7). If these dimers exist *in vivo* at all, their stability is expected to be low, considering that no bilateral co-depletions corresponding to Rrp41/42-like dimers were observed.

While the exosome assembly model offers insights into association of catalytic subunits, whether the complex is already catalytic active upon association remains unclear. Also, whether binding of adapter complexes required for exosome activity is adversely affected by Exosc1 depletion remains to be determined.

All experiments were done using mESCs and conservation of observations to other cell types and animals might be limited. It seems plausible that complex formation would be highly conserved given the strong selective pressure to maintain a functional complex. While Exosc1 is not required for essential exosome functions in mESCs, this might not be the case in other organisms or tissues, where it might play a specialized role in RNA metabolism. KOs of Exosc1 are also seemingly not compatible with viable development in mice as preweaning mortality of Exosc1 KO mice has been reported by the International Mouse Phenotyping Consortium (111,112).

7 Outlook

While the inducible Cas9 KO system was used to provide preliminary evidence for Exosc1 dispensability for some exosome complex functions and to elucidate exosome complex assembly *in vivo*, many open questions remain.

For example, it is formally not known at what stage Dis3 or adapter complexes like Ski, NEXT and PAXT can associate with the exosome core. Additionally, the extent and nature of exosome functions maintained in absence of Exosc1 remain partially elusive. How and at what stage of assembly the exosome is imported to the nucleus has yet to be addressed. Further, higher homogeneity and penetrance of KOs might improve resolution of molecular phenotypes and could be achieved by improving the Tet-On Cas9 system.

7.1 Improved inducible Cas9 system

As discussed previously, the inducible Cas9 system could be optimized to avoid Cas9 and rtTA silencing, which is likely limiting KO penetrance. To this end, an all-in-one vector could be used for FRT mediated targeted integration of rtTA and Cas9 to the Rosa26 locus which is ubiquitously expressed in mice (105).

In this construct, rtTA expression could be translationally coupled through an internal ribosome entry site (IRES) to a hygromycin resistance gene. This would already provide an advantage over the current system where rtTA and hygromycin resistance are expressed from different promoters. The rtTA-IRES-hygro^R would be separated with a TRE containing promoter through a dual insulator sequence to avoid promoter interference as described previously (113). The TRE promoter would control the expression of Cas9 coupled through a P2A-site to iRFP713, a far-red fluorescent protein. In sum, expression of Cas9 and rtTA from the Rosa26 locus and direct coupling of rtTA expression to hygromycin resistance should greatly reduce silencing.

In growth competition experiments, falling relative cell numbers can be due to cell cycle arrest or apoptosis and the two cannot be resolved currently. Removal of eYFP and BFP from the system and instead expression of a far-red protein would open possibilities for further FACS based measurements. Specifically, growth competitions experiments (mCherry based) as described here could be combined with cell cycle and viability measurements. For example, DAPI and Annexin V co-staining could be done to distinguish healthy, early, and late apoptotic cells using the currently occupied blue (BFP, DAPI) and yellow/green (eYFP, Annexin V antibodies) spectra. Such experiments could be set up in high throughput and each sample would contain its own negative control, since WT cells would be mixed with KO cells and distinguishable from them by lack of mCherry signal.

So far, such an all-in-one recombination construct has been cloned and successfully integrated to the Rosa26 locus. Currently, clonal cell lines are being established and validated in the lab. Using this system in the future could reduce noise due to a more controlled genetic background and increase KO penetrance due to lack of silencing as well as enabling more informative growth competitions screens as discussed.

7.2 Confirmation of the assembly model

To confirm and more precisely quantify factor co-depletions, KOs of specific factors could be subjected to mass spectrometry. Co-immunoprecipitation of exosome complexes from induced KOs could prove the existence of subcomplexes. For this purpose, pulling on either component of the Exosc2/4/7 trimer should allow to purify any proposed subcomplex. However, this would only prove the existence of proposed subcomplexes *in vitro*.

Complex assembly is arrested at a specific stage in the absence of any component and thus any assembly co-factors that associate with the complex at this specific stage could be co-purified. However, whether such cofactors exist is unclear since exosome assembly *in vitro* is possible by combining purified core subunits (10,20). Additionally, Co-IPs of partially assembled exosomes may be used to address association of adapter complexes like the Ski, NEXT or PAXT complexes as well as nucleases at certain stages of complex assembly.

Co-IPs could serve to further characterize Exosc1 devoid exosomes. Interaction of nuclear adapter complexes as well as Dis3 and Dis3L with the Exosc1 devoid exosome are expected as discussed. Furthermore, potential binding of Exosc10 to the Exosc1 devoid exosomes could be investigated. While Exosc1 is expected to greatly enhance Exosc10 recruitment to the complex, it is conceivable that Exosc10 could to some degree still interact with the exosome in absence of Exosc1. Thus, quantification of exosome bound Exosc10 may further aid understanding of Exosc1's function in exosome biology.

7.3 Molecular phenotyping of Exosc1 KOs

While pulldowns may serve to elucidate which co-factors can association with the exosome at any given step in the assembly, this is no prove of functionality. Instead, testing the abundance of nuclear and cytoplasmic exosome targets in Exosc1 KO cells may elucidate the role of Exosc1 in exosome function. Specifically, levels of known nuclear targets like PROMPTs and cytoplasmic targets like histone mRNA could be addressed by qPCR (41,58).

Potentially, the sole function of Exosc1 could be to mediate Exosc10 exosome dependent functions. If Exosc1 is required for Exosc10 mediated exosome activity, differences in molecular phenotypes of Exosc1 KOs could be compared to Exosc10 KOs to characterize Exosc10 exosome independent functions.

The exosome plays an important role in stem cell differentiation (72). Thus, examination of the differentiation potential of mESCs lacking Exosc1 could provide new insights. Furthermore, Exosc1 could be knocked out in other cell lines to determine if Exosc1 viability is mESC specific. Additionally, Exosc1 may perform tissue specific functions hence differences caused by Exosc1 depletions in different cell lines could be assessed.

7.4 Import of the Exosome complex to the nucleus

Mechanism and assembly state that enables exosome import to the nucleus remains unclear. It was proposed that import might be facilitated by association with the NLS containing proteins Exosc10 and Dis3 (110). Exosc10 is unlikely to be solely responsible for

nuclear exosome import, since Exosc10 interactions with the exosome are highly dependent on Exosc1 and Exosc1 KOs are viable (Fig. 6A-B) (20).

First, inducible single and double KOs of Dis3 and Exosc10 could be generated, and complex localization could be assessed by cellular fractionation and Western blot. Thereby, it could be determined whether either is necessary or sufficient for import.

Should there still be a substantial fraction of exosome core subunits found in the nucleus, the localization of the Exosc2/4/7 trimer could be assessed in Exosc6 KOs. If the trimer would be found in the nucleus still, complex formation could likely occur in the cytoplasm or nucleus. However, if depletion of Exosc6 led to a depletion of Exosc2/4/7 from the nucleus, likely only larger subcomplexes or fully assembled exosomes can be imported. Nuclear import could then be assessed in different KOs, determining at which stage of complex assembly import is possible.

Finally, if nuclear import would be Dis3 and Exosc10 independent and relying on (sub-) complex formation, there might be a specialized import factor mediating the import. Screening for such a factor could be achieved by doing a KO-screen that uses nuclear exosome activity as a readout. For this purpose, upregulation of specific nuclear targets might be used as a readout with FISH to discover genes needed for import.

8 Materials and Methods

Experimental procedures are described as indicated. Equipment, buffers, cell lines and sequences are specified under "8.9 Materials".

8.1 Tissue culture

The mESC cell line used in all experiments was the An3-12 cell line obtained from IMBA Haplobank. Cells were kept at 37 °C and 5 % CO_2 in high-glucose DMEM containing 1x Penicillin-Streptomycin (20 U/ 100 mL Penicillin, 20 µg/ 100 mL Streptomycin), 2 mM L-Glutamine, 15 % FCS, 1 mM Sodium Pyruvate, 1x non-essential amino acids, 50 µM 2-Mercaptoethanol and 2 µg/ 100 mL LIF. Hygromycin selection was done prior to Cas9 induction for at least seven days by adding 250 µg/mL hygromycin B. Selection for sgRNA plasmid expressing cells was done by adding 1 µg/mL puromycin for three to five days. Cells were split 1:8 – 1:10 at 80 % confluency every 48 h following trypsinization. Cells in 24-well plate were kept at RT for 15 minutes after splitting and resuspended again to avoid cluster formation in the center or periphery of the wells.

8.2 Generating the inducible Cas9 cell line

The inducible Cas9 system was generated and established previously by Tsimafei Navalayeu. In short, random lentiviral integration a plasmid encoding SFFV-rtTA and PGK-hygro^R done to the genome of Tir1-eYFP, Xrn1-AID expressing An3-12 cells. Following hygromycin treatment before TRE-Cas9-P2A-BFP was integrated. Single cells expressing BFP following doxycycline induction were grown to full clonal populations and a cell line with non-leaky, but inducible Cas9 expression was chosen for further experimentation.

8.3 Viral sgRNA vectors and oligonucleotides

The design of sgRNA sequences was done by Robert Kalis, MSc and based on the VBC score (100). Two sgRNAs were designed per targeted gene (for sequences see 8.9 Materials) and cloned into LentiCRISPRv2 plasmids (Addgene plasmid # 52961) as previously described (101,114). In short, sense and antisense oligos were ordered with specific 3′ and/or 5′ sequences for cloning. Specifically, sense sgRNA1 oligos had a 3′ CACC sequence and sgRNA1 antisense oligos had a 5′ CAAA sequence, sgRNA2 sense oligos contained a 3′ CTTGTTT and a 3′ GTTTA sequence and sgRNA2 antisense oligos had a 3′ AAA and 5′ CAAATTCTC sequence. Oligos with complementary sgRNA sequences were annealed and phosphorylated. sgRNA1 oligos were mixed with the LentiCRISPRv2 plasmid, both were digested with Esp3I and ligated with T4 DNA ligase. Then sgRNA2 oligos were added to the reaction with BbsI and ligated into the backbone. Reaction mix was used to transform Stbl3 chemically competent cells. Purified plasmids were submitted to Sanger Sequencing to confirm correct sgRNA sequence before using them for Lentivirus production. The expression of the sgRNAs was under the control of a human and a mouse U6 promoter and a separate EF1a core promoter drove expression of mCherry-P2A-puro^R.

8.4 Lentivirus production

Virus packaging LentiX cells (HEK293(F)T cells) were kept at 37 °C and 5 % CO_2 in high-glucose DMEM containing 2 mM L-Glutamine, 10 % FCS, 1 mM Sodium Pyruvate, 1x non-essential amino acids and 50 µM 2-Mercaptoethanol. Cells were stained with

Trypan Blue and counted using Nexcelom Cellometer Auto 2000 Cell Viability Counter. 50.000 – 100.000 cells were seeded per 24-well plate well or 250.000 – 500.000 cells per 6-well plate well 24 h before transfection. Cells were transfected at 70 - 80 % confluency with the following transfection mix:

	6-well plate	24-well plate
Opti-Mem	200 µL	40 µL
pCMV	1140 ng	228 ng
pVSV-G	670 ng	134 ng
transfection vector (e.g. sgRNA plasmid)	2300 ng	460 ng
PEI	12 µL	2.4 µL

Transfection mix was vortexed and incubated for 25 min at RT. Transfection mix was added dropwise and transfection medium was exchanged to target medium 3 - 12 h after adding. Virus was harvested 24 - 30 h afterwards and filtered with 0.45 µm filter when obtained from 6-well plates. Virus from 24-well plates was not filtered, but instead the virus containing supernatant was frozen to kill any remaining packaging cells.

mESCs (An3-12) were infected at 70 – 80 % confluency with virus containing medium and 10 ng/mL polybrene (final concentration). 24 h after infection, medium was exchanged, and selection was started with 1 µg/mL puromycin.

8.5 Viability assays

A Luciferase Assay (Promega) was used to determine cell viability and doxycycline toxicity according to the manufacturer's protocol. In short, cells were seeded in 96-well plates and treated with doxycycline, an untreated control was kept and cells corresponding to one well were killed by heat immediately. After 24 h, cells were washed with 1x PBS and dispensed in 20 µL lysis reactant. 100 µL Luciferase Assay Reagent was added to each well and the emitted light was measured with a plate reader (Szabo Scandic Synergy H1). Signal from heat-killed cells was subtracted and signal from each sample was normalized to the untreated control.

8.6 Western blotting and image quantification

Western blotting was done as described previously (115,116). Cells were pelleted, pellets were lysed with lysis buffer containing 150 mM NaCl, 1 % Triton X-100, 0.5 % Sodium deoxycholate, 0.1 % SDS, 50 mM Tris-HCl pH 8.0 and 1x protease inhibitor cocktail. The lysate was incubated on ice for 30 minutes and spun down at 25.000 x g, 4 °C for 20 minutes. The supernatant containing total protein lysate was kept.

A Bradford assay to evaluate the protein concentration was performed according to the provider's manual. 80 – 200 µg protein (varying between experiments) were mixed with loading buffer and denatured at 95 °C for 5 minutes.

Separating gels with 12 % or a gradient from 8 % - 16 % acrylamide and pH 8.7 were cast with stacking gels with 6.8 pH and 5 % acrylamide. Gels were run at 50 – 100 V until the samples had reached the separating gel, then voltage was increased to 100 – 200 V.

The gel was stopped once the 15 kDa band of the marker had run out of the gel. Transfer to a PVDF membrane was done at 4 °C with 55 V for 4 h or overnight.

Alternatively, precast gradient gels were loaded and run as described and transfer was performed either for 1 h at 100 V at 4 °C or by diffusion blotting over 48 h to two membranes as described previously (117).

Membranes were stained with Ponceau staining solution and cut between the 75 kDa and 100 kDa bands as well as the 37 kDa and 50 kDa bands. Since staining did not work after diffusion transfer, one marker was loaded in the first and last well and a straight cut was made between the two at appropriate sizes. Membranes were blocked with 3 % milk at RT for 20 minutes.

Incubation with primary antibody was done o/n at 4 °C and following five 1-minute TBST wash steps, secondary antibodies were added for at least 1 h at RT. Primary antibodies were kept at 4 °C in 3 % milk with sodium azide and reused multiple times. After washing the membranes with TBST they were incubated for 1 minute with ECL staining solution and imaged (ChemiDoc).

Image analysis was done using Fiji taking into account the linear range of chemiluminescence signal (104,118). This was done by quantifying the values of the dilution series. To assess the linearity, which may be lost at any point of the dilution series, values were normalized to the amount of protein loaded at this dilution and divided by the next higher normalized dilution. This can be expressed in the following formula:

$$Q_n = (x_n * 100 / n) / (x_p * 100 / p)$$

n…. Protein dilution (100 %, 50 %, 25 %, 10 %, 5 %)
p…. Previous dilution (100 %, 50 %, 25 %, 10 %)
Q_n… Linearity quality factor of n
x_n… Background subtracted value of n
x_p… Background subtracted value of p

Thus, linearity between any two dilutions was quantified without the need for plotting a graph which may underestimate the loss of linearity at lower dilutions and makes it difficult to objectively judge quality and range of linearity. Here, linearity was deemed sufficient for quantification based on the arbitrarily chosen threshold $Q_n = 1 \pm 0.3$.

Linearity might be lost gradually between multiple dilution steps which would distort Q_n, since each dilution is compared to the one before, which might already be biased. Therefore, a second measure was used to assess linearity between any dilution and the 50 % mark.

$$Q_{n50} = 50 / n * x_n / x_{50}$$

n…… Protein dilution (100 %, 50 %, 25 %, 10 %, 5 %)
Q_{n50}… Linearity quality factor of n
x_{50}….. Background subtracted value of dilution at 50 %
x_n….. Background subtracted value of n

In this way, linearity between any two dilutions is quantified in relationship to the 50 % dilution. Here linearity was deemed sufficient for quantification if $Q_{n50} = \pm 0.3$, a cutoff that was chosen arbitrarily.

Generally, Q_n or $Q_{n50} > 1$ indicate that the signal of this dilution was too high in relationship to the next higher or 50 % dilution and vice versa.

For example, linearity is lost in the Exosc10 dilution series from replicate #2 of Exosc4 KOs at higher dilutions (Supplementary Fig. S14A). Thus, high values cannot be quantified accurately, however linear loss of signal from 50 % to 5 % was observed and thus absolute values in this range may be quantified accurately. This was suitable for quantification of Exosc10 signal in Exosc4 KOs, which was at 8 % after 72 h.

In the Hsp70 dilution series from replicate #2 of Exosc4 KOs, loss of signal at lower dilution values can be observed (Supplementary Fig. S14B). The loss of linearity is not obvious from when values are plotted, but Q_n and Q_{n50} illustrate that sufficient linearity is only observed between the 100 % and 50 % dilutions. In this case the samples' signals were in this range, so quantification could be done normally. In cases where the signal was lower, a linear range between the two lowest dilutions was assumed and the sample's value was normalized accordingly.

8.7 Flow cytometry

Flow cytometry was performed with IntelliCyt iQue Screener and BD LSR Fortessa™ Cell Analyzer with HTS module. All flow cytometry experiments were done with 96- well plates and samples were measured in technical triplicates. For excitation of eYFP the 488 nm laser and for mCherry the 561 nm laser was used.

8.8 Illustrations

Illustrations were created with biorender.com.

8.9 Materials

Equipment and buffers	Provider and Details (if applicable)
2-Mercaptoethanol	Sigma-Aldrich 2-Mercaptoethanol, ≥99.0 % (M6250-100ML)
Acrylamide	Sigma Aldrich Ultra pure Protogel 30 % (w/v) Acrylamide/ 0.8 % Bis-acrylamide (w/v)
Ammoniumpersulfate (APS)	Biozyme (903001)
Anti- Actin antibodies	Sigma Aldrich Anti-Actin antibody produced in rabbit (A2066-.2ML)
Anti- Dis3 antibodies	Proteintech Dis3 Antibody (14689-1-AP), 1000x rabbit
Anti- Dis3L antibodies	Santa Cruz Biotechnology DIS3L (E-12) Antibodies (sc-398739), 100x, from mouse
Anti- Exosc1 antibodies	Bethyl Laboratories (A303-885A-T), 2000x, from rabbit

Anti- Exosc2 antibodies	Proteintech Exosc2 polyclonal antibodies, 5000x, from rabbit (14805-1-AP)
Anti- Exosc3 antibodies #1	Novus Biologicals Polyclonal Polyclonal Exosc3 antibodies (NBP2-22261), from rabbit, 1000x; strong unspecific band observed slightly above Exosc3 band
Anti- Exosc3 antibodies #2	Proteintech Exosc3 polyclonal antibodies, from rabbit (15062-1-AP), 1000x
Anti- Exosc4 antibodies	Proteintech Exosc4 polyclonal antibodies from rabbit (15062-1-AP), 1000x
Anti- Exosc5 antibodies	Proteintech Exosc5 polyclonal antibody from rabbit (15627-1-AP), 5000x
Anti- Exosc6 antibodies	Santa Cruz Biotechnology EXOSC6 monoclonal antibody from mouse (sc-398277), 1000x
Anti- Exosc7 antibodies	Santa Cruz Biotechnology EXOSC7 monoclonal Antibody (A-1) from mouse (sc-393686), 1000x
Anti- Exosc8 antibodies	Proteintech Exosc8 polyclonal antibody from rabbit (11979-1-AP), 5000x
Anti- Exosc9 antibodies	Santa Cruz Biotechnology EXOSC9 (D-6) monoclonal antibodies from mouse (sc-271815), 1000x
Anti- Exosc10 antibodies	Santa Cruz Biotechnology EXOSC10 (B-8) monoclonal antibodies from mouse (sc-374595), 1000x
Anti- Hsp70 antibodies	Abcam Hsp70 monoclonal antibodies (5A5) from mouse (ab2787), 1000x
Anti- mouse IgG antibodies	Thermo Fisher Goat anti-Mouse IgG (H+L) Secondary Antibody, HRP conjugate (G21040), 10.000x
Anti- Mtr4 antibodies	Abcam anti-Mtr4 antibody from rabbit (ab70551), 1000x
Anti- rabbit IgG antibodies	Invitrogen Goat anti-Rabbit IgG (H+L) Secondary Antibody, HRP conjugate (G21234), 10.000x
BbsI	BbsI-HF®, New England Biolabs, Size=1,500 units (R3539L)
Cell counter	Nexcelom Cellometer Auto 2000 Cell Viability Counter
Cell counting slip	Nexcelom Cellometer SD100
Dishes (10cm, 6-well, 24-well, 96-well)	Thermo Scientific Nunclon MultiDishes
DMEM high glucose	Provided by in-house media kitchen; DMEM F12 11.996 g/L HEPES FOR CELL CULTURE 3.575 g/L SODIUM BICARBONATE 2.43g/L pH 7.2-7.4; sterile filtered
Doxycyclin	Sigma Aldrich Doxycycline hyclate (D9891)
Dry Milk Powder	Dissolved to 3 % (w/v) for membrane blocking; Maresi

ECL solution	Biorad Clarity Western ECL Substrate (170-5060)
Esp3I	New England Biolabs (NEB) Esp3i - 1,500 units (R0734L)
Ethanol	Brenntag Ethanol S96 % UG 1L Petrolether (458619)
FBS	Sigma Aldrich Sterile filtered fetal calf serum (F7524); Batch tested by in-house stem cell facility
Flow Cytometer	IntelliCyt iQue Screener, BD LSR Fortessa™ Cell Analyzer with HTS module
Flow cytometry analysis software	FlowJo™ Software v10
Hygromycin B	Roche Hygromycin B, 50 mg/mL (10843555001)
Image Analysis Software	Fiji; see Schindelin et al. (118)
L-Glutamine	Gibco™ L-Glutamine, 200mM (11539876)
LentiGuide-Puro Vector	Addgene plasmid #52961; http://n2t.net/addgene:52961; RRID: Addgene_52961
LentiX cells	HEK293(F)T cells; gifted by Dr. Moritz Staltner
LIF	Provided by in-house Molecular Biology Service facility
Lipofectamine	ThermoFisher Lipofectamine 3000 Reagent (L3000001)
Loading Buffer (SDS)	1x buffer contains 62.5 mM Tris-HCl pH 6.8, 2.5 % SDS, 0.002 % Bromophenol Blue, 0.7135 M (5 %) β-mercaptoethanol, 10 % glycerol; stock was 6x concentrated
Luciferase Assay Kit	Promega CellTiter-Glo Luminescent Cell Viability Assay (G7571)
Cell Lysis buffer (Protein extraction)	NaCl 150mM Triton X-100 1 % Sodium deoxycholate 0.5 % SDS 0.1 % Tris-HCl pH 8.0, 50 mM
mESCs	An3-12 cells obtained from haplobank.at, Cell ID: 00000WA00
NanoDrop	Thermo Scientific NanoDrop™ 2000c Spectrophotometer
Non-essential amino acids	Gibco™ MEM Non-essential Amino Acid Solution (100x), liquid, without L-glutamine, sterile-filtered, cell culture
PBS	Provided by in-house media kitchen; 1x stock POTASSIUM CHLORIDE 0.2 g/L POTASSIUM PHOSPHATE MONOBASIC 0.2 g/L Sodium Chloride 8 g/L

	SODIUM PHOSPHATE DIBASIC 1.15 g/L
pCMV	Addgene 12260
Penicillin-Streptomycin	Gibco™ Penicillin-Streptomycin-Glutamin, 100x (12090216)
Plate reader	Szabo Scandic Synergy H1 Hybrid Reader 3
Polybrene	Milipore Polybrene Transfection Reagent, 10 mg/mL (TR-1003-G)
Polyethylenimine (PEI)	Polyethylenimine, Linear (MW 25,000); 9 mg/mL
Ponceau staining solution	Sigma Aldrich (6226-79-5)
Precast Acrylamide Gels	4–15 % and 4-20 % Mini-PROTEAN® TGX™ Precast Protein Gels, 10 and 20-well
Protease inhibitor	Thermo Scientific Halt Protease Inhibitor Cocktail, EDTA-free (100X) (87785)
Protein ladder	Biorad Precision Plus Protein Dual Color Standards
Puromycin	Gibco™Puromycin Dihydrochloride 10 mg/mL (A1113803)
PVDF Membrane	EMD Millipore Immobilon-P Membrane, PVDF, 0.45µm (IPVH00010)
pVSVg	Addgene 8454
SDS PAGE Running Equipment	Bio-Rad Mini Trans-Blot Cell (1703930)
SDS running buffer	Provided by in-house media kitchen; 10x stock Glycine 149.6 g/L SDS BioChemica 10 g/L Trizma® base 30.2 g/L
Sodium Azide	Sigma Aldrich Sodium Azide (S2002-25G)
Sodium dodecyl sulfate (SDS)	Ambion (AM9820)
Sodium Pyruvate	Gibco Sodium Pyruvate 100x (11360070)
Stbl3 cells	Chemically competent; provided by in-house Molecular Biology Serivce facility
T4 DNA Ligase	New England Biolabs T4 DNA Ligase (M0202M)
TBST	TBS provided by in-house media kitchen; 0.5 M Tris pH 7.5 1.67 M NaCl 0.1 % Tween-20 added separately
TEMED	Pierce™ TEMED, Thermo Scientific (17919)
Tris-HCl Buffer for stacking gel	1 M Tris-HCl pH 6.8
Tris-HCl Buffer for separating gel	1.5 M Tris-HCl pH 8.7
Triton X-100	Sigma Aldrich (T8787-100ML)
Trypan Blue	Thermo Scientific Trypan Blue Stain (0.4 %) (T10282)
Trypsin	Gibco™ Trypsin-EDTA (0.5 %), no phenol red, 100x (15400054)
Tween-20	Sigma Aldrich, Tween-20 (655205-250)
Western Blot Imaging System	Bio-Rad ChemiDoc Imaging System

Western Blot Stripping Solution	VWR Restore Western Blot Stripping Buffer (PIER21063)
Western Blot Transfer Buffer	provided by in-house media kitchen w/o alcohol; 10x stock Glycine 131.25 g/L Trizma® base 28.125 g/L 1x buffer contained 10 % Ethanol
Western Blot Transfer Equipment	Bio-Rad Mini Trans-Blot Module (1703935)

Targeted gene	**sgRNA sequence (fwd)**
Dis3 sgRNA1	GCAGGGAAAATTATTTGG
Dis3 sgRNA2	GCATAGAATGAAATAGAAAGT
Dis3L #2 sgRNA1	GATCCTAGCCAACCACTGGG
Dis3L #2 sgRNA2	GCGGCCCAGGAACTACTGGA
Exosc1 sgRNA1	GATGTAGCCATGCCGGGTGT
Exosc1 sgRNA2	GGGGATGCAGTACCTCAC
Exosc1 #2 sgRNA1	TAGGAACTCGGGCTGTACTCGGG
Exosc1 #2 sgRNA2	TGAAAAGAGCTGGGCGTGTGG
Exosc1 #3 sgRNA1	GGGAGCTGTCGTCACCTGTAAGG
Exosc1 #3 sgRNA2	TGAAAAGAGCTGGGCGTGTGG
Exosc1 #4 sgRNA1	TCGGCCAGGTGACATAGTTTTGG
Exosc1 #4 sgRNA2	TCCCACATCTGGACAACTGGG
Exosc2 sgRNA1	GGTCGGAGACATTGTAGTG
Exosc2 sgRNA2	GTCATCCATGAACCTACCTGG
Exosc3 sgRNA1	GATCACTATGCCAATCACG
Exosc3 sgRNA2	GTCTTACCTGGCATTTGAAG
Exosc3 sgRNA1	GATCACTATGCCAATCACG
Exosc3 sgRNA2	GTCTTACCTGGCATTTGAAG
Exosc4 sgRNA1	GCAGCTACGACAGACCTTCG
Exosc4 sgRNA2	GGATGCTGGGATACCTATGC
Exosc5 sgRNA1	GGCCTCAGGATCACTTCA
Exosc5 sgRNA2	GCCTGGCTGGAGTCTATGGGC
Exosc6 sgRNA1	GCAAGGGCTCCGCCTACCTGG
Exosc6 sgRNA2	GACCGGAGAAGGGAGCGCGG
Exosc7 sgRNA1	GCTGGAGAAACCGAATGA
Exosc7 sgRNA2	GCCACGGCCATCCACCCGA
Exosc8 sgRNA1	GTGAAGCTGGGGAATACCA
Exosc8 sgRNA2	GAGCCACAACTGTCAACAT
Exosc9 sgRNA1	GTGAAGAACGAGTAATGGA
Exosc9 sgRNA2	GATAATGCTGCTTAAAGACC
Exosc10 sgRNA1	GGGACGACACCAAGTGGCA
Exosc10 sgRNA2	GAAGGTACCTCTAAGTCCA
Olfr10 sgRNA1	TAGGAAGAGCTACAGTCACAGGG
Olfr10 sgRNA2	ACCTTCAATATCAGTTTGGGAGG
Olfr23 sgRNA1	GAGGTTTGGGCTCATGATTCTGG

Olfr23 sgRNA2	GAATGAGGACAATGATGACGAGG
Olfr55 sgRNA1	GAACATGACAAGTAAAATGGTGG
Olfr55 sgRNA2	ACCCATGACAGTGAGTAGAAAGG
Skiv2l sgRNA1	GCACGTTCAGCAGCTCCCAA
Skiv2l sgRNA2	GTTCAGGGGATCTAGGGG
Ttc37 sgRNA1	GGACTATGTGGAACAAGCGC
Ttc37 sgRNA2	GCATCTCCCACGAGCTTCCAA
Wdr61 sgRNA1	GAACGCAACATTCAACACCC
Wdr61 sgRNA2	GAAAAGGTCAAGGAGCGAAT
Xrn1 sgRNA1	GAAGGAGAGCATAAAATCA
Xrn1 sgRNA2	GTCCACAGACAAATCATGGCA

Only sense sgRNA sequences are given. In all cases oligos with complementary antisense sequences were ordered including specific sgRNA1 and sgRNA2 sense and antisense nucleotides for cloning (see 8.3 Viral vectors and oligonucleotides).

9 Acknowledgements

I would like to express my gratitude to my thesis advisor Prof. Dr. Stefan Ameres of the University of Vienna's Max Perutz Labs (MPL) for the opportunity to work on this exciting project, as well as for his mentorship, insights, and helpful discussions.

Additionally, I would like to thank Specialist Tsimafei Navalayeu for sharing his project and enthusiasm with me, for being a patient and supportive instructor and a good friend. While allowing this thesis to be my own work, he provided guidance whenever needed.

Further, I would like to thank the core facilities, particularly the FACS facility of the Institute of Molecular Pathology (IMP) and our lab technicians Ivica Sowemimo, MSc and Monika Ducka, PhD, who went out of their way to provide everything needed for successful experiments. Moreover, I would like to thank Robert Kalis, MSc for designing the sgRNAs.

Lastly, I would like to thank all my colleagues, particularly current and previous members of the Ameres lab for their companionship, humor and, generating a great work environment, by sharing know-how, ideas, and the occasional beer.

10 References

1. Januszyk K, Lima CD. The eukaryotic RNA exosome. Curr Opin Struct Biol. 2014 Feb;24:132–40.

2. Allmang C, Petfalski E, Podtelejnikov A, Mann M, Tollervey D, Mitchell P. The yeast exosome and human PM-Scl are related complexes of 3' right-arrow 5' exonucleases. Genes Dev. 1999 Aug 15;13(16):2148–58.

3. Briggs MW, Burkard KTD, Butler JS. Rrp6p, the Yeast Homologue of the Human PM-Scl 100-kDa Autoantigen, Is Essential for Efficient 5.8 S rRNA 3′ End Formation. J Biol Chem. 1998 May;273(21):13255–63.

4. Kim DU, Hayles J, Kim D, Wood V, Park HO, Won M, et al. Analysis of a genome-wide set of gene deletions in the fission yeast Schizosaccharomyces pombe. Nat Biotechnol. 2010 Jun;28(6):617–23.

5. Mitchell P, Petfalski E, Shevchenko A, Mann M, Tollervey D. The Exosome: A Conserved Eukaryotic RNA Processing Complex Containing Multiple 3′→5′ Exoribonucleases. Cell. 1997 Nov;91(4):457–66.

6. Morton DJ, Kuiper EG, Jones SK, Leung SW, Corbett AH, Fasken MB. The RNA exosome and RNA exosome-linked disease. RNA N Y N. 2018 Feb;24(2):127–42.

7. Wasmuth EV, Lima CD. Structure and Activities of the Eukaryotic RNA Exosome. The Enzymes. 2012;31:53–75.

8. Houseley J, LaCava J, Tollervey D. RNA-quality control by the exosome. Nat Rev Mol Cell Biol. 2006 Jul;7(7):529–39.

9. Mitchell P, Petfalski E, Tollervey D. The 3' end of yeast 5.8S rRNA is generated by an exonuclease processing mechanism. Genes Dev. 1996 Feb 15;10(4):502–13.

10. Liu Q, Greimann JC, Lima CD. Reconstitution, activities, and structure of the eukaryotic RNA exosome. Cell. 2006 Dec 15;127(6):1223–37.

11. Shi Z, Yang WZ, Lin-Chao S, Chak KF, Yuan HS. Crystal structure of *Escherichia coli* PNPase: Central channel residues are involved in processive RNA degradation. RNA. 2008 Nov;14(11):2361–71.

12. Symmons MF, Jones GH, Luisi BF. A Duplicated Fold Is the Structural Basis for Polynucleotide Phosphorylase Catalytic Activity, Processivity, and Regulation. Structure. 2000 Nov;8(11):1215–26.

13. Büttner K, Wenig K, Hopfner KP. Structural Framework for the Mechanism of Archaeal Exosomes in RNA Processing. Mol Cell. 2005 Nov;20(3):461–71.

14. Lorentzen E, Walter P, Fribourg S, Evguenieva-Hackenberg E, Klug G, Conti E. The archaeal exosome core is a hexameric ring structure with three catalytic subunits. Nat Struct Mol Biol. 2005 Jul;12(7):575–81.

15. Navarro MVAS, Oliveira CC, Zanchin NIT, Guimarães BG. Insights into the Mechanism of Progressive RNA Degradation by the Archaeal Exosome. J Biol Chem. 2008 May;283(20):14120–31.

16. Evguenieva-Hackenberg E, Walter P, Hochleitner E, Lottspeich F, Klug G. An exosome-like complex in *Sulfolobus solfataricus*. EMBO Rep. 2003 Sep;4(9):889–93.

17. Evguenieva-Hackenberg E, Hou L, Glaeser S, Klug G. Structure and function of the archaeal exosome: Structure and function of the archaeal exosome. Wiley Interdiscip Rev RNA. 2014 Sep;5(5):623–35.

18. Dziembowski A, Lorentzen E, Conti E, Séraphin B. A single subunit, Dis3, is essentially responsible for yeast exosome core activity. Nat Struct Mol Biol. 2007 Jan;14(1):15–22.

19. Tomecki R, Kristiansen MS, Lykke-Andersen S, Chlebowski A, Larsen KM, Szczesny RJ, et al. The human core exosome interacts with differentially localized processive RNases: hDIS3 and hDIS3L. EMBO J. 2010 Jul 21;29(14):2342–57.

20. Makino DL, Baumgärtner M, Conti E. Crystal structure of an RNA-bound 11-subunit eukaryotic exosome complex. Nature. 2013 Mar;495(7439):70–5.

21. Zinder JC, Wasmuth EV, Lima CD. Nuclear RNA Exosome at 3.1 Å Reveals Substrate Specificities, RNA Paths, and Allosteric Inhibition of Rrp44/Dis3. Mol Cell. 2016 Nov;64(4):734–45.

22. Zuo Y. Exoribonuclease superfamilies: structural analysis and phylogenetic distribution. Nucleic Acids Res. 2001 Mar 1;29(5):1017–26.

23. Allmang C. Functions of the exosome in rRNA, snoRNA and snRNA synthesis. EMBO J. 1999 Oct 1;18(19):5399–410.

24. Chang HM, Triboulet R, Thornton JE, Gregory RI. A role for the Perlman syndrome exonuclease Dis3l2 in the Lin28–let-7 pathway. Nature. 2013 May;497(7448):244–8.

25. Malecki M, Viegas SC, Carneiro T, Golik P, Dressaire C, Ferreira MG, et al. The exoribonuclease Dis3L2 defines a novel eukaryotic RNA degradation pathway. EMBO J. 2013 Mar 15;32(13):1842–54.

26. Reimão-Pinto MM, Manzenreither RA, Burkard TR, Sledz P, Jinek M, Mechtler K, et al. Molecular basis for cytoplasmic RNA surveillance by uridylation-triggered decay in *Drosophila*. EMBO J. 2016 Nov 15;35(22):2417–34.

27. Lebreton A, Tomecki R, Dziembowski A, Séraphin B. Endonucleolytic RNA cleavage by a eukaryotic exosome. Nature. 2008 Dec;456(7224):993–6.

28. Robinson S, Oliver A, Chevassut T, Newbury S. The 3’ to 5’ Exoribonuclease DIS3: From Structure and Mechanisms to Biological Functions and Role in Human Disease. Biomolecules. 2015 Jul 17;5(3):1515–39.

29. Wasmuth EV, Lima CD. Exo- and Endoribonucleolytic Activities of Yeast Cytoplasmic and Nuclear RNA Exosomes Are Dependent on the Noncatalytic Core and Central Channel. Mol Cell. 2012 Oct;48(1):133–44.

30. Januszyk K, Liu Q, Lima CD. Activities of human RRP6 and structure of the human RRP6 catalytic domain. RNA. 2011 Aug;17(8):1566–77.

31. Callahan KP, Butler JS. Evidence for core exosome independent function of the nuclear exoribonuclease Rrp6p. Nucleic Acids Res. 2008 Dec;36(21):6645–55.

32. Bonneau F, Basquin J, Ebert J, Lorentzen E, Conti E. The Yeast Exosome Functions as a Macromolecular Cage to Channel RNA Substrates for Degradation. Cell. 2009 Oct;139(3):547–59.

33. Hardwick SW, Luisi BF. Rarely at rest: RNA helicases and their busy contributions to RNA degradation, regulation and quality control. RNA Biol. 2013 Jan;10(1):56–70.

34. Mitchell P. Exosome substrate targeting: the long and short of it. Biochem Soc Trans. 2014 Aug 1;42(4):1129–34.

35. Weick EM, Lima CD. RNA helicases are hubs that orchestrate exosome-dependent 3′–5′ decay. Curr Opin Struct Biol. 2021 Apr;67:86–94.

36. Weick EM, Puno MR, Januszyk K, Zinder JC, DiMattia MA, Lima CD. Helicase-Dependent RNA Decay Illuminated by a Cryo-EM Structure of a Human Nuclear RNA Exosome-MTR4 Complex. Cell. 2018 Jun;173(7):1663-1677.e21.

37. Gerlach P, Schuller JM, Bonneau F, Basquin J, Reichelt P, Falk S, et al. Distinct and evolutionary conserved structural features of the human nuclear exosome complex. eLife. 2018 Jul 26;7:e38686.

38. Lubas M, Christensen MS, Kristiansen MS, Domanski M, Falkenby LG, Lykke-Andersen S, et al. Interaction Profiling Identifies the Human Nuclear Exosome Targeting Complex. Mol Cell. 2011 Aug;43(4):624–37.

39. Meola N, Domanski M, Karadoulama E, Chen Y, Gentil C, Pultz D, et al. Identification of a Nuclear Exosome Decay Pathway for Processed Transcripts. Mol Cell. 2016 Nov;64(3):520–33.

40. Coy S, Volanakis A, Shah S, Vasiljeva L. The Sm Complex Is Required for the Processing of Non-Coding RNAs by the Exosome. Kanai A, editor. PLoS ONE. 2013 Jun 6;8(6):e65606.

41. Kilchert C, Wittmann S, Vasiljeva L. The regulation and functions of the nuclear RNA exosome complex. Nat Rev Mol Cell Biol. 2016 Apr;17(4):227–39.

42. Lubas M, Andersen PR, Schein A, Dziembowski A, Kudla G, Jensen TH. The Human Nuclear Exosome Targeting Complex Is Loaded onto Newly Synthesized RNA to Direct Early Ribonucleolysis. Cell Rep. 2015 Jan;10(2):178–92.

43. Wu Y, Liu W, Chen J, Liu S, Wang M, Yang L, et al. Nuclear Exosome Targeting Complex Core Factor Zcchc8 Regulates the Degradation of LINE1 RNA in Early Embryos and Embryonic Stem Cells. Cell Rep. 2019 Nov;29(8):2461-2472.e6.

44. Silla T, Schmid M, Dou Y, Garland W, Milek M, Imami K, et al. The human ZC3H3 and RBM26/27 proteins are critical for PAXT-mediated nuclear RNA decay. Nucleic Acids Res. 2020 Mar 18;48(5):2518–30.

45. Bühler M, Haas W, Gygi SP, Moazed D. RNAi-dependent and -independent RNA turnover mechanisms contribute to heterochromatic gene silencing. Cell. 2007 May 18;129(4):707–21.

46. Kadaba S, Wang X, Anderson JT. Nuclear RNA surveillance in Saccharomyces cerevisiae: Trf4p-dependent polyadenylation of nascent hypomethylated tRNA and an aberrant form of 5S rRNA. RNA N Y N. 2006 Mar;12(3):508–21.

47. Meola N, Jensen TH. Targeting the nuclear RNA exosome: Poly(A) binding proteins enter the stage. RNA Biol. 2017 Jul 3;14(7):820–6.

48. Puno MR, Weick EM, Das M, Lima CD. SnapShot: The RNA Exosome. Cell. 2019 Sep;179(1):282-282.e1.

49. San Paolo S, Vanacova S, Schenk L, Scherrer T, Blank D, Keller W, et al. Distinct roles of non-canonical poly(A) polymerases in RNA metabolism. PLoS Genet. 2009 Jul;5(7):e1000555.

50. Thiebaut M, Kisseleva-Romanova E, Rougemaille M, Boulay J, Libri D. Transcription termination and nuclear degradation of cryptic unstable transcripts: a role for the nrd1-nab3 pathway in genome surveillance. Mol Cell. 2006 Sep 15;23(6):853–64.

51. Tudek A, Porrua O, Kabzinski T, Lidschreiber M, Kubicek K, Fortova A, et al. Molecular basis for coordinating transcription termination with noncoding RNA degradation. Mol Cell. 2014 Aug 7;55(3):467–81.

52. Wlotzka W, Kudla G, Granneman S, Tollervey D. The nuclear RNA polymerase II surveillance system targets polymerase III transcripts. EMBO J. 2011 May 4;30(9):1790–803.

53. Pefanis E, Wang J, Rothschild G, Lim J, Kazadi D, Sun J, et al. RNA exosome-regulated long non-coding RNA transcription controls super-enhancer activity. Cell. 2015 May 7;161(4):774–89.

54. Xue Z, Yuan H, Guo J, Liu Y. Reconstitution of an Argonaute-dependent small RNA biogenesis pathway reveals a handover mechanism involving the RNA exosome and the exonuclease QIP. Mol Cell. 2012 May 11;46(3):299–310.

55. Staals RHJ, Bronkhorst AW, Schilders G, Slomovic S, Schuster G, Heck AJR, et al. Dis3-like 1: a novel exoribonuclease associated with the human exosome. EMBO J. 2010 Jul 21;29(14):2358–67.

56. Garneau NL, Wilusz J, Wilusz CJ. The highways and byways of mRNA decay. Nat Rev Mol Cell Biol. 2007 Feb;8(2):113–26.

57. Łabno A, Tomecki R, Dziembowski A. Cytoplasmic RNA decay pathways - Enzymes and mechanisms. Biochim Biophys Acta. 2016 Dec;1863(12):3125–47.

58. Tuck AC, Rankova A, Arpat AB, Liechti LA, Hess D, Iesmantavicius V, et al. Mammalian RNA Decay Pathways Are Highly Specialized and Widely Linked to Translation. Mol Cell. 2020 Mar;77(6):1222-1236.e13.

59. Chen CY, Gherzi R, Ong SE, Chan EL, Raijmakers R, Pruijn GJM, et al. AU Binding Proteins Recruit the Exosome to Degrade ARE-Containing mRNAs. Cell. 2001 Nov;107(4):451–64.

60. Conti E, Izaurralde E. Nonsense-mediated mRNA decay: molecular insights and mechanistic variations across species. Curr Opin Cell Biol. 2005 Jun;17(3):316–25.

61. Doma MK, Parker R. Endonucleolytic cleavage of eukaryotic mRNAs with stalls in translation elongation. Nature. 2006 Mar;440(7083):561–4.

62. Frischmeyer PA, van Hoof A, O'Donnell K, Guerrerio AL, Parker R, Dietz HC. An mRNA Surveillance Mechanism That Eliminates Transcripts Lacking Termination Codons. Science. 2002 Mar 22;295(5563):2258–61.

63. van Hoof A, Frischmeyer PA, Dietz HC, Parker R. Exosome-Mediated Recognition and Degradation of mRNAs Lacking a Termination Codon. Science. 2002 Mar 22;295(5563):2262–4.

64. Boczonadi V, Müller JS, Pyle A, Munkley J, Dor T, Quartararo J, et al. EXOSC8 mutations alter mRNA metabolism and cause hypomyelination with spinal muscular atrophy and cerebellar hypoplasia. Nat Commun. 2014 Sep;5(1):4287.

65. Di Donato N, Neuhann T, Kahlert AK, Klink B, Hackmann K, Neuhann I, et al. Mutations in *EXOSC2* are associated with a novel syndrome characterised by retinitis pigmentosa, progressive hearing loss, premature ageing, short stature, mild intellectual disability and distinctive gestalt. J Med Genet. 2016 Jun;53(6):419–25.

66. Rudnik-Schoneborn S, Senderek J, Jen JC, Houge G, Seeman P, Puchmajerova A, et al. Pontocerebellar hypoplasia type 1: Clinical spectrum and relevance of EXOSC3 mutations. Neurology. 2013 Jan 29;80(5):438–46.

67. Wan J, Yourshaw M, Mamsa H, Rudnik-Schöneborn S, Menezes MP, Hong JE, et al. Mutations in the RNA exosome component gene EXOSC3 cause pontocerebellar hypoplasia and spinal motor neuron degeneration. Nat Genet. 2012 Jun;44(6):704–8.

68. de Groen FLM, Krijgsman O, Tijssen M, Vriend LEM, Ylstra B, Hooijberg E, et al. Gene-dosage dependent overexpression at the 13q amplicon identifies *DIS3* as candidate oncogene in colorectal cancer progression: 13q Gain in CRC Progression. Genes Chromosomes Cancer. 2014 Apr;53(4):339–48.

69. Lohr JG, Stojanov P, Carter SL, Cruz-Gordillo P, Lawrence MS, Auclair D, et al. Widespread Genetic Heterogeneity in Multiple Myeloma: Implications for Targeted Therapy. Cancer Cell. 2014 Jan;25(1):91–101.

70. Ng D, Toure O, Wei MH, Arthur DC, Abbasi F, Fontaine L, et al. Identification of a novel chromosome region, 13q21.33-q22.2, for susceptibility genes in familial chronic lymphocytic leukemia. Blood. 2007 Feb 1;109(3):916–25.

71. Weißbach S, Langer C, Puppe B, Nedeva T, Bach E, Kull M, et al. The molecular spectrum and clinical impact of *DIS3* mutations in multiple myeloma. Br J Haematol. 2015 Apr;169(1):57–70.

72. Fraga de Andrade I, Mehta C, Bresnick EH. Post-transcriptional control of cellular differentiation by the RNA exosome complex. Nucleic Acids Res. 2020 Dec 2;48(21):11913–28.

73. Mistry DS, Chen Y, Sen GL. Progenitor Function in Self-Renewing Human Epidermis is Maintained by the Exosome. Cell Stem Cell. 2012 Jul;11(1):127–35.

74. Pefanis E, Basu U. RNA Exosome Regulates AID DNA Mutator Activity in the B Cell Genome. In: Advances in Immunology [Internet]. Elsevier; 2015 [cited 2022 Jun 19]. p. 257–308. Available from: https://linkinghub.elsevier.com/retrieve/pii/S0065277615000322

75. Skamagki M, Zhang C, Ross CA, Ananthanarayanan A, Liu Z, Mu Q, et al. RNA Exosome Complex-Mediated Control of Redox Status in Pluripotent Stem Cells. Stem Cell Rep. 2017 Oct;9(4):1053–61.

76. Ishino Y, Shinagawa H, Makino K, Amemura M, Nakata A. Nucleotide sequence of the iap gene, responsible for alkaline phosphatase isozyme conversion in Escherichia coli, and identification of the gene product. J Bacteriol. 1987 Dec;169(12):5429–33.

77. Mojica FJM, Juez G, Rodriguez-Valera F. Transcription at different salinities of Haloferax mediterranei sequences adjacent to partially modified PstI sites. Mol Microbiol. 1993 Aug;9(3):613–21.

78. Bolotin A, Quinquis B, Sorokin A, Ehrlich SD. Clustered regularly interspaced short palindrome repeats (CRISPRs) have spacers of extrachromosomal origin. Microbiology. 2005 Aug 1;151(8):2551–61.

79. Mojica FJM, D□ez-Villase□or C, Garc□a-Mart□nez J, Soria E. Intervening Sequences of Regularly Spaced Prokaryotic Repeats Derive from Foreign Genetic Elements. J Mol Evol. 2005 Feb;60(2):174–82.

80. Pourcel C, Salvignol G, Vergnaud G. CRISPR elements in Yersinia pestis acquire new repeats by preferential uptake of bacteriophage DNA, and provide additional tools for evolutionary studies. Microbiology. 2005 Mar 1;151(3):653–63.

81. Barrangou R, Fremaux C, Deveau H, Richards M, Boyaval P, Moineau S, et al. CRISPR Provides Acquired Resistance Against Viruses in Prokaryotes. Science. 2007 Mar 23;315(5819):1709–12.

82. Ishino Y, Krupovic M, Forterre P. History of CRISPR-Cas from Encounter with a Mysterious Repeated Sequence to Genome Editing Technology. Margolin W, editor. J Bacteriol [Internet]. 2018 Apr [cited 2022 Mar 26];200(7). Available from: https://journals.asm.org/doi/10.1128/JB.00580-17

83. Shmakov S, Smargon A, Scott D, Cox D, Pyzocha N, Yan W, et al. Diversity and evolution of class 2 CRISPR–Cas systems. Nat Rev Microbiol. 2017 Mar;15(3):169–82.

84. Garneau JE, Dupuis MÈ, Villion M, Romero DA, Barrangou R, Boyaval P, et al. The CRISPR/Cas bacterial immune system cleaves bacteriophage and plasmid DNA. Nature. 2010 Nov 4;468(7320):67–71.

85. Gasiunas G, Barrangou R, Horvath P, Siksnys V. Cas9–crRNA ribonucleoprotein complex mediates specific DNA cleavage for adaptive immunity in bacteria. Proc Natl Acad Sci [Internet]. 2012 Sep 25 [cited 2022 Mar 27];109(39). Available from: https://pnas.org/doi/full/10.1073/pnas.1208507109

86. Mojica FJM, Díez-Villaseñor C, García-Martínez J, Almendros C. Short motif sequences determine the targets of the prokaryotic CRISPR defence system. Microbiology. 2009 Mar 1;155(3):733–40.

87. Liao C, Beisel CL. The tracrRNA in CRISPR Biology and Technologies. Annu Rev Genet. 2021 Nov 23;55(1):161–81.

88. Deltcheva E, Chylinski K, Sharma CM, Gonzales K, Chao Y, Pirzada ZA, et al. CRISPR RNA maturation by trans-encoded small RNA and host factor RNase III. Nature. 2011 Mar;471(7340):602–7.

89. Sander JD, Joung JK. CRISPR-Cas systems for editing, regulating and targeting genomes. Nat Biotechnol. 2014 Apr;32(4):347–55.

90. Popp MW, Maquat LE. Leveraging Rules of Nonsense-Mediated mRNA Decay for Genome Engineering and Personalized Medicine. Cell. 2016 Jun;165(6):1319–22.

91. Tuladhar R, Yeu Y, Tyler Piazza J, Tan Z, Rene Clemenceau J, Wu X, et al. CRISPR-Cas9-based mutagenesis frequently provokes on-target mRNA misregulation. Nat Commun. 2019 Dec;10(1):4056.

92. El-Brolosy MA, Stainier DYR. Genetic compensation: A phenomenon in search of mechanisms. PLoS Genet. 2017 Jul;13(7):e1006780.

93. Khalil AM. The genome editing revolution: review. J Genet Eng Biotechnol. 2020 Oct 29;18(1):68.

94. Gossen M, Freundlieb S, Bender G, Müller G, Hillen W, Bujard H. Transcriptional Activation by Tetracyclines in Mammalian Cells. Science. 1995 Jun 23;268(5218):1766–9.

95. Zhang J, Chen L, Zhang J, Wang Y. Drug Inducible CRISPR/Cas Systems. Comput Struct Biotechnol J. 2019;17:1171–7.

96. Gossen M, Bujard H. Tight control of gene expression in mammalian cells by tetracycline-responsive promoters. Proc Natl Acad Sci. 1992 Jun 15;89(12):5547–51.

97. Zhou X, Vink M, Klaver B, Berkhout B, Das AT. Optimization of the Tet-On system for regulated gene expression through viral evolution. Gene Ther. 2006 Oct;13(19):1382–90.

98. Zhou J, Wang J, Shen B, Chen L, Su Y, Yang J, et al. Dual sgRNAs facilitate CRISPR/Cas9-mediated mouse genome targeting. FEBS J. 2014 Apr;281(7):1717–25.

99. Sanjana NE, Shalem O, Zhang F. Improved vectors and genome-wide libraries for CRISPR screening. Nat Methods. 2014 Aug;11(8):783–4.

100. Michlits G, Jude J, Hinterndorfer M, de Almeida M, Vainorius G, Hubmann M, et al. Multilayered VBC score predicts sgRNAs that efficiently generate loss-of-function alleles. Nat Methods. 2020 Jul;17(7):708–16.

101. de Almeida M, Hinterndorfer M, Brunner H, Grishkovskaya I, Singh K, Schleiffer A, et al. AKIRIN2 controls the nuclear import of proteasomes in vertebrates. Nature. 2021 Nov;599(7885):491–6.

102. Schwanhäusser B, Busse D, Li N, Dittmar G, Schuchhardt J, Wolf J, et al. Global quantification of mammalian gene expression control. Nature. 2011 May 19;473(7347):337–42.

103. Estévez AM, Lehner B, Sanderson CM, Ruppert T, Clayton C. The Roles of Intersubunit Interactions in Exosome Stability. J Biol Chem. 2003 Sep;278(37):34943–51.

104. Pillai-Kastoori L, Schutz-Geschwender AR, Harford JA. A systematic approach to quantitative Western blot analysis. Anal Biochem. 2020 Mar;593:113608.

105. Friedrich G, Soriano P. Promoter traps in embryonic stem cells: a genetic screen to identify and mutate developmental genes in mice. Genes Dev. 1991 Sep;5(9):1513–23.

106. Schaeffer D, Tsanova B, Barbas A, Reis FP, Dastidar EG, Sanchez-Rotunno M, et al. The exosome contains domains with specific endoribonuclease, exoribonuclease and cytoplasmic mRNA decay activities. Nat Struct Mol Biol. 2009 Jan;16(1):56–62.

107. Dai L, Zhao T, Bisteau X, Sun W, Prabhu N, Lim YT, et al. Modulation of Protein-Interaction States through the Cell Cycle. Cell. 2018 May;173(6):1481-1494.e13.

108. Malet H, Topf M, Clare DK, Ebert J, Bonneau F, Basquin J, et al. RNA channelling by the eukaryotic exosome. EMBO Rep. 2010 Dec;11(12):936–42.

109. Wang HW, Wang J, Ding F, Callahan K, Bratkowski MA, Butler JS, et al. Architecture of the yeast Rrp44–exosome complex suggests routes of RNA recruitment for 3′ end processing. Proc Natl Acad Sci. 2007 Oct 23;104(43):16844–9.

110. Rech B, Gonzales-Zubiate FA. Mechanisms of Nuclear Transport in the cell: RNA exosome in Saccharomyces cerevisiae. Bionatura. 2020 Nov 15;5(4):1423–6.

111. Elrick H, Peterson KA, Wood JA, Lanza DG, Acar EF, Teboul L, et al. The production of 4,182 mouse lines identifies experimental and biological variables impacting Cas9-mediated mutant mouse line production [Internet]. Genetics; 2021 Oct [cited 2022 Jun 30]. Available from: http://biorxiv.org/lookup/doi/10.1101/2021.10.06.463037

112. The International Mouse Phenotyping Consortium, Dickinson ME, Flenniken AM, Ji X, Teboul L, Wong MD, et al. High-throughput discovery of novel developmental phenotypes. Nature. 2016 Sep 22;537(7621):508–14.

113. Haenebalcke L, Goossens S, Naessens M, Kruse N, Ghahremani MF, Bartunkova S, et al. Efficient ROSA26-Based Conditional and/or Inducible Transgenesis Using RMCE-Compatible F1 Hybrid Mouse Embryonic Stem Cells. Stem Cell Rev Rep. 2013 Dec;9(6):774–85.

114. Umkehrer C, Holstein F, Formenti L, Jude J, Froussios K, Neumann T, et al. Isolating live cell clones from barcoded populations using CRISPRa-inducible reporters. Nat Biotechnol. 2021 Feb;39(2):174–8.

115. Renart J, Reiser J, Stark GR. Transfer of proteins from gels to diazobenzyloxymethyl-paper and detection with antisera: a method for studying antibody specificity and antigen structure. Proc Natl Acad Sci. 1979 Jul;76(7):3116–20.

116. Yang PC, Mahmood T. Western blot: Technique, theory, and trouble shooting. North Am J Med Sci. 2012;4(9):429.

117. Olsen I, Wiker HG. Diffusion blotting for rapid production of multiple identical imprints from sodium dodecyl sulfate polyacrylamide gel electrophoresis on a solid support. J Immunol Methods. 1998 Nov;220(1–2):77–84.

118. Schindelin J, Arganda-Carreras I, Frise E, Kaynig V, Longair M, Pietzsch T, et al. Fiji: an open-source platform for biological-image analysis. Nat Methods. 2012 Jun 28;9(7):676–82.

11 Supplementary figures

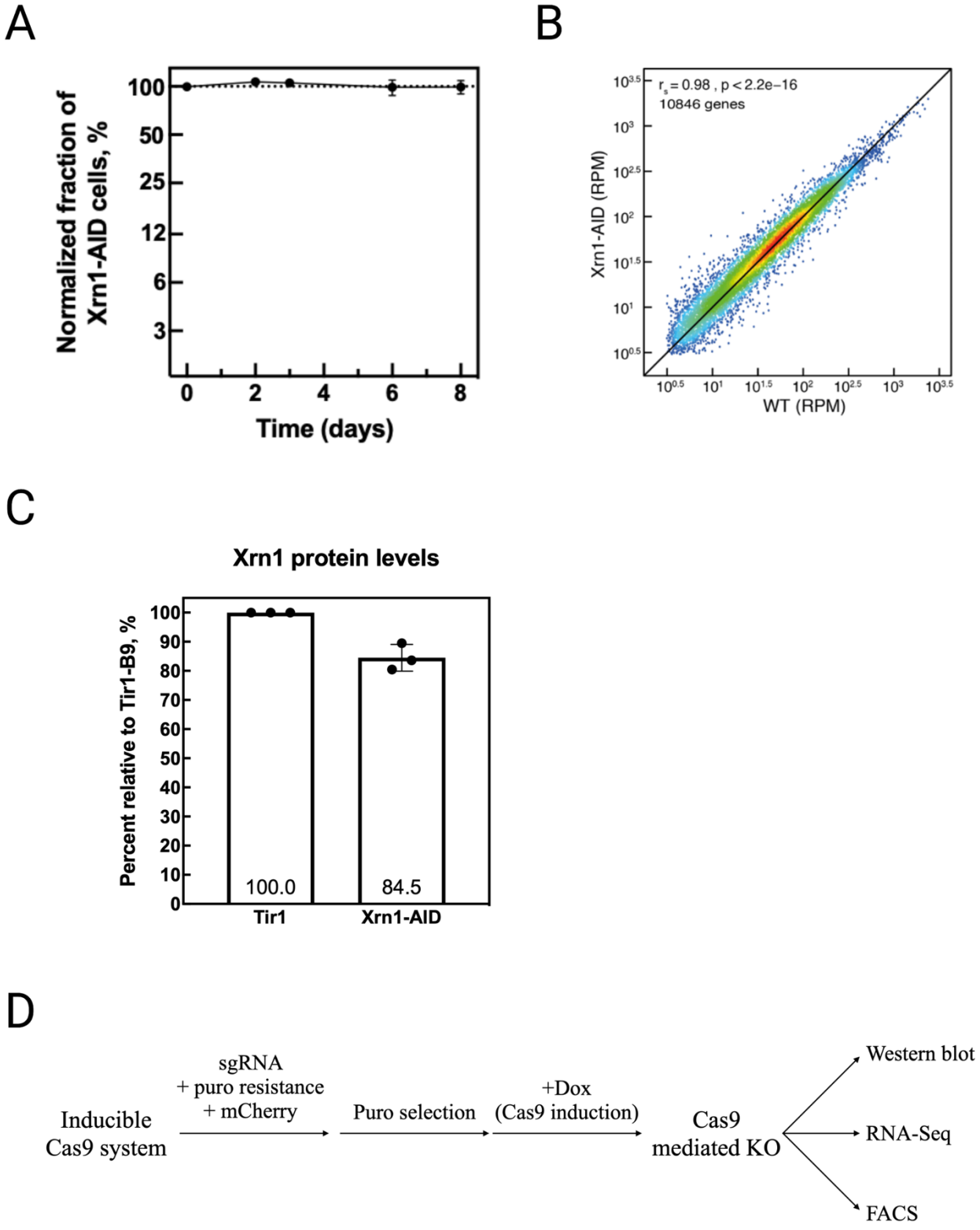

Supplementary Figure S1: (**A**) Growth competition of Xrn1-AID cell compared to WT cells. (**B**) RNA-Seq of WT and Xrn1-AID. (**C**) Protein levels of Xrn1 before and after AID tagging. (**D**) Schematics of workflow generating a Cas9 inducible KO. sgRNA is integrated together with puromycin (puro) resistance and mCherry. Following puromycin selection, Cas9 is induced by addition of doxycycline (dox) and phenotypes are read out.

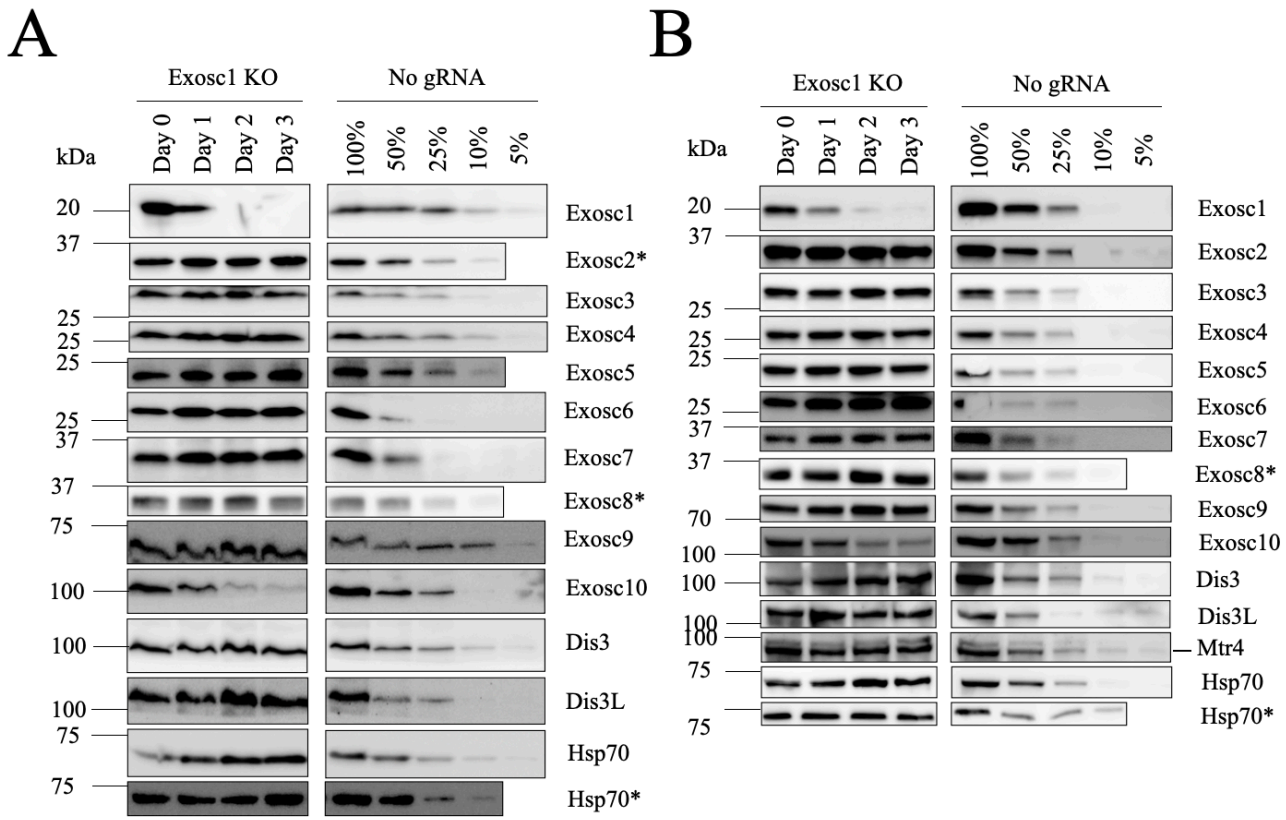

Supplementary Figure S2: Western blots of Exosc1 KO time courses, imaged to assess levels of exosome subunits. Asterisks indicate respective loading control. (**A**) Replicate 1. (**B**) Replicate 2, including nuclear helicase Mtr4. Different Exosc3 antibodies were used than in (A) to avoid unspecific band.

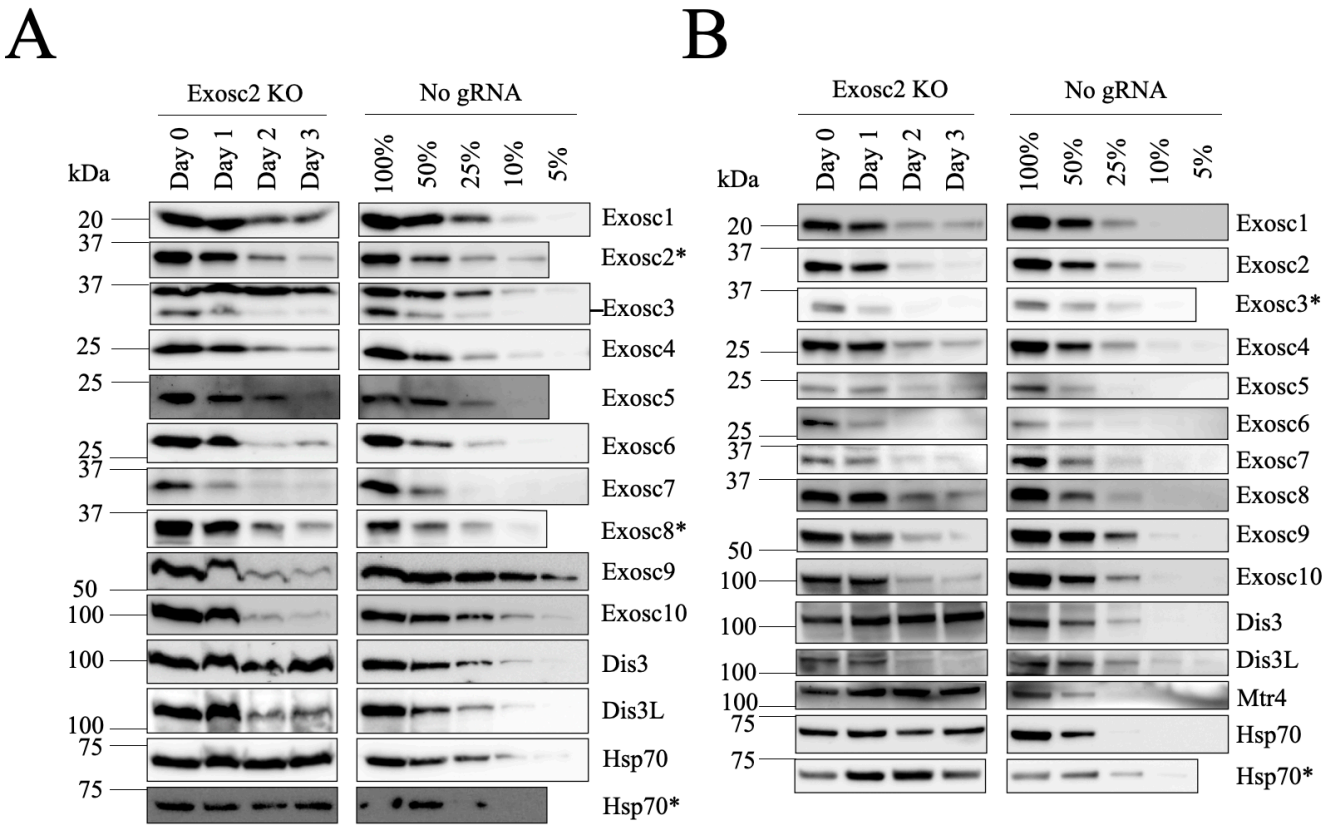

Supplementary Figure S3: Western blots of Exosc2 KO time courses, imaged to assess levels of exosome subunits. (**A**) Replicate 1. (**B**) Replicate 2, including nuclear helicase Mtr4. Different Exosc3 antibodies were used than in (A) to avoid unspecific band.

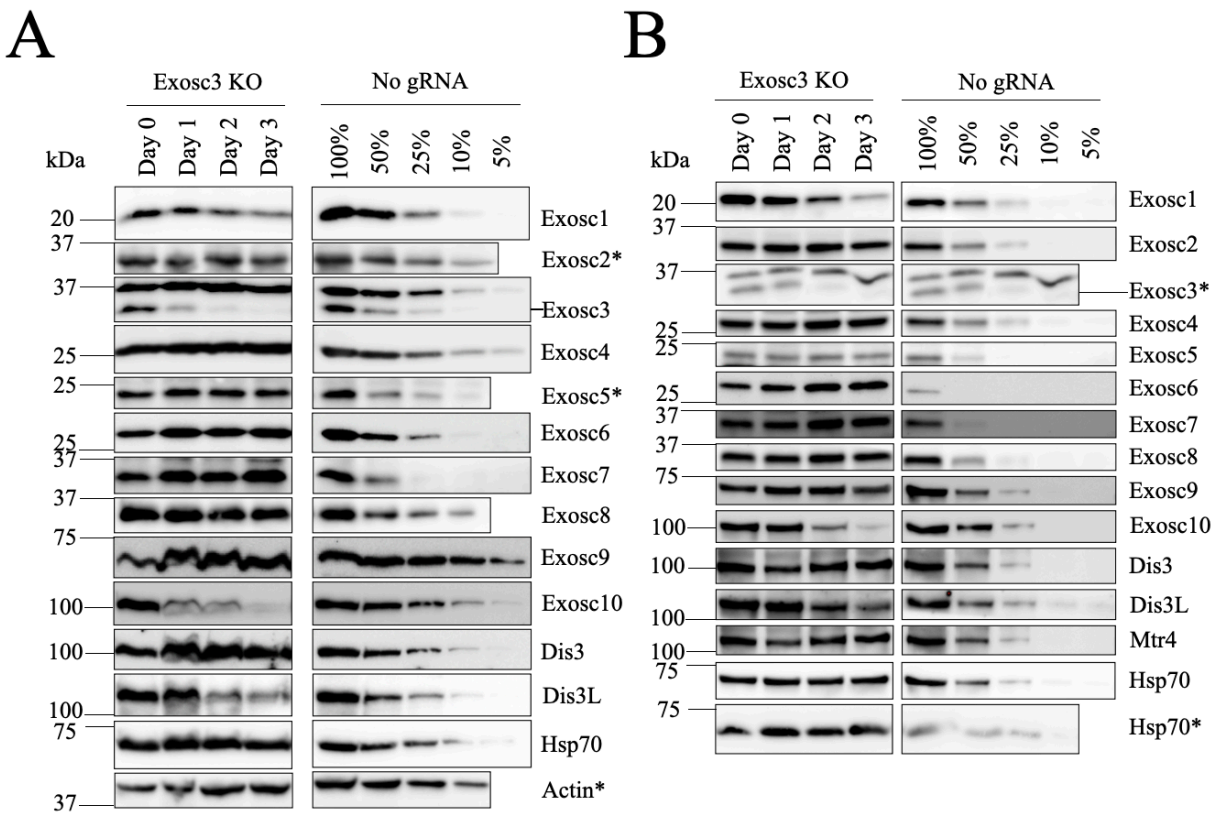

Supplementary Figure S4: Western blots of Exosc3 KO time courses, imaged to assess levels of exosome subunits. Asterisks indicate respective loading control. (**A**) Replicate 1. (**B**) Replicate 2, includes nuclear helicase Mtr4.

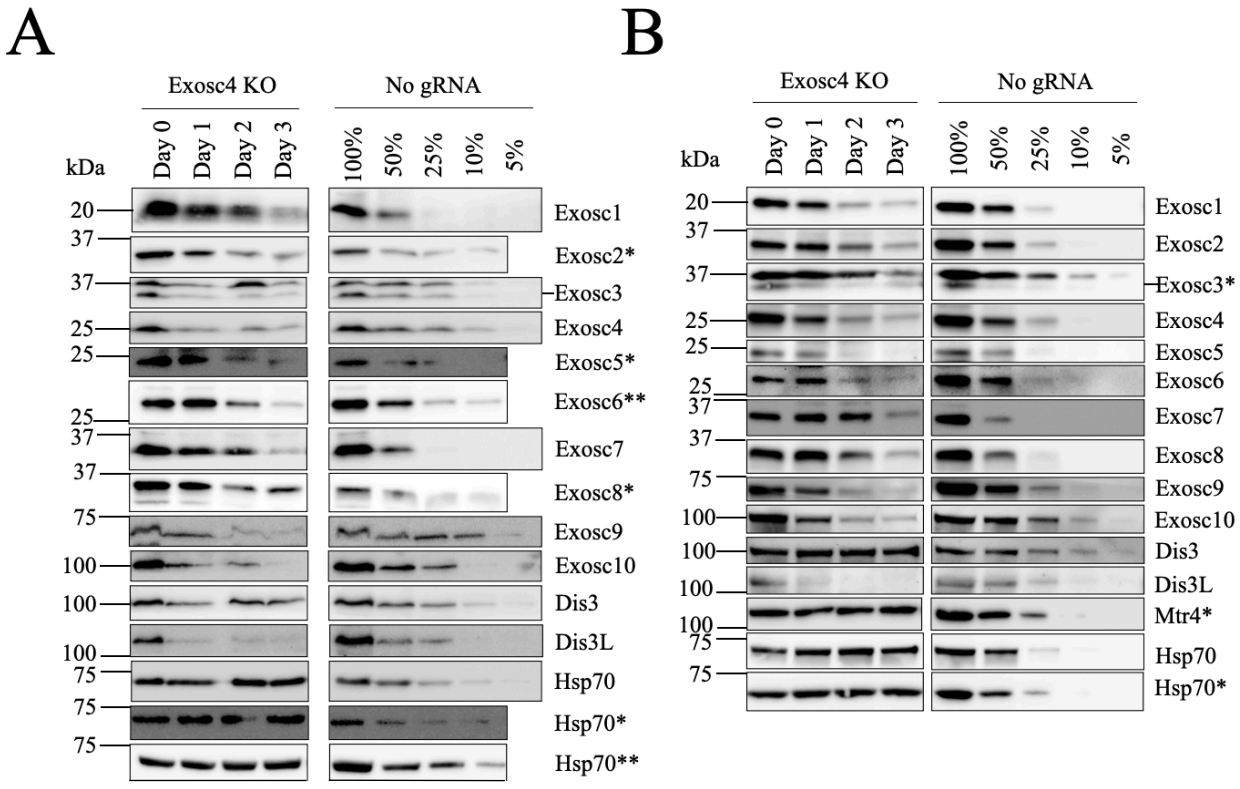

Supplementary Figure S5: Western blots of Exosc4 KO time courses, imaged to assess levels of exosome subunits. Asterisks indicate respective loading control. (**A**) Replicate 1. (**B**) Replicate 2, including nuclear helicase Mtr4.

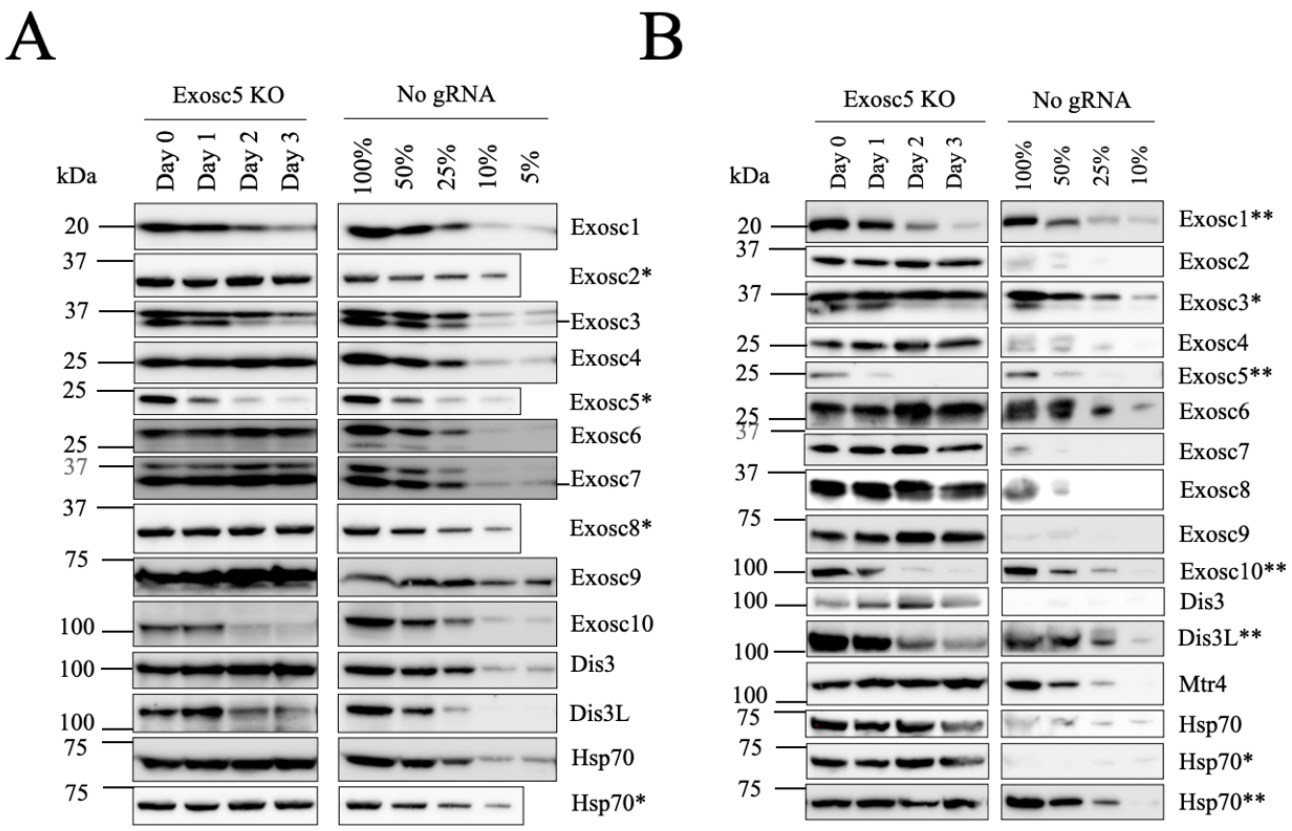

Supplementary Figure S6: Western blots of Exosc5 KO time courses, imaged to assess levels of exosome subunits. Asterisks indicate respective loading control. (**A**) Replicate 1. (**B**) Replicate 2, including nuclear helicase Mtr4.

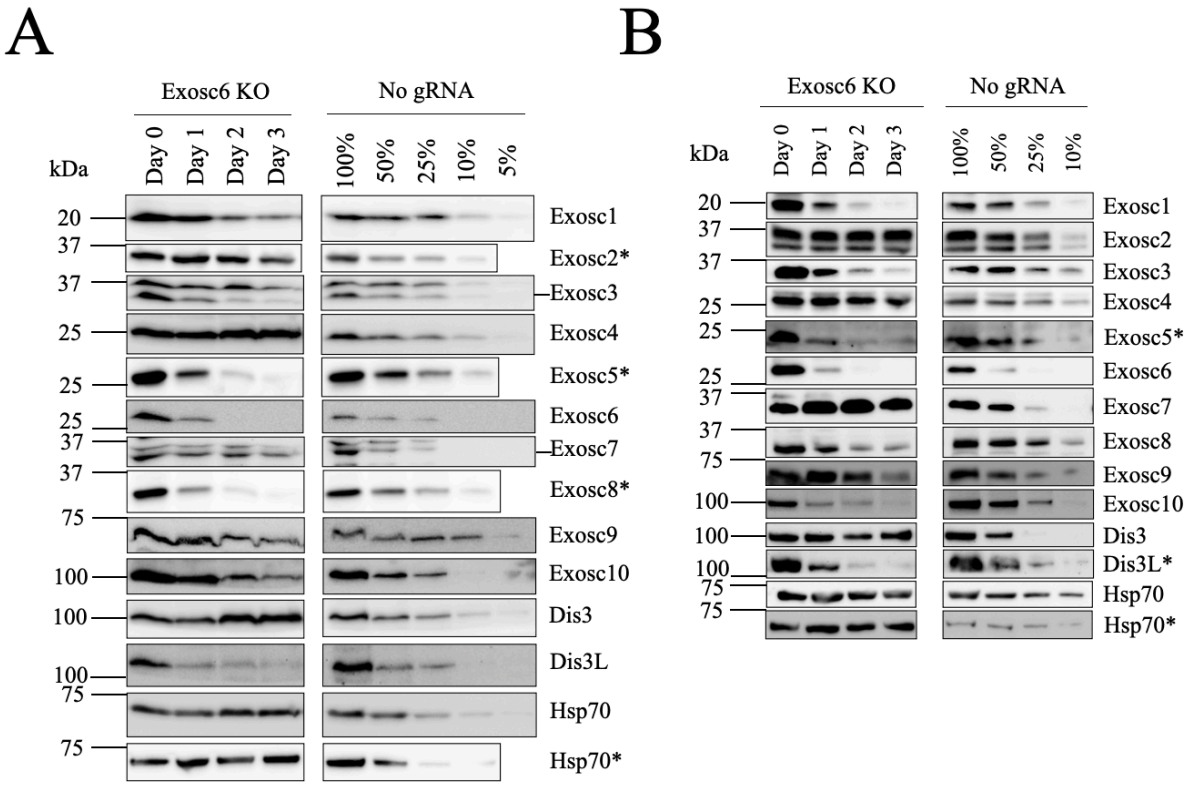

Supplementary Figure S7: Western blots of Exosc6 KO time courses, imaged to assess levels of exosome subunits. Asterisks indicate respective loading control. (**A**) Replicate 1. (**B**) Replicate 2.

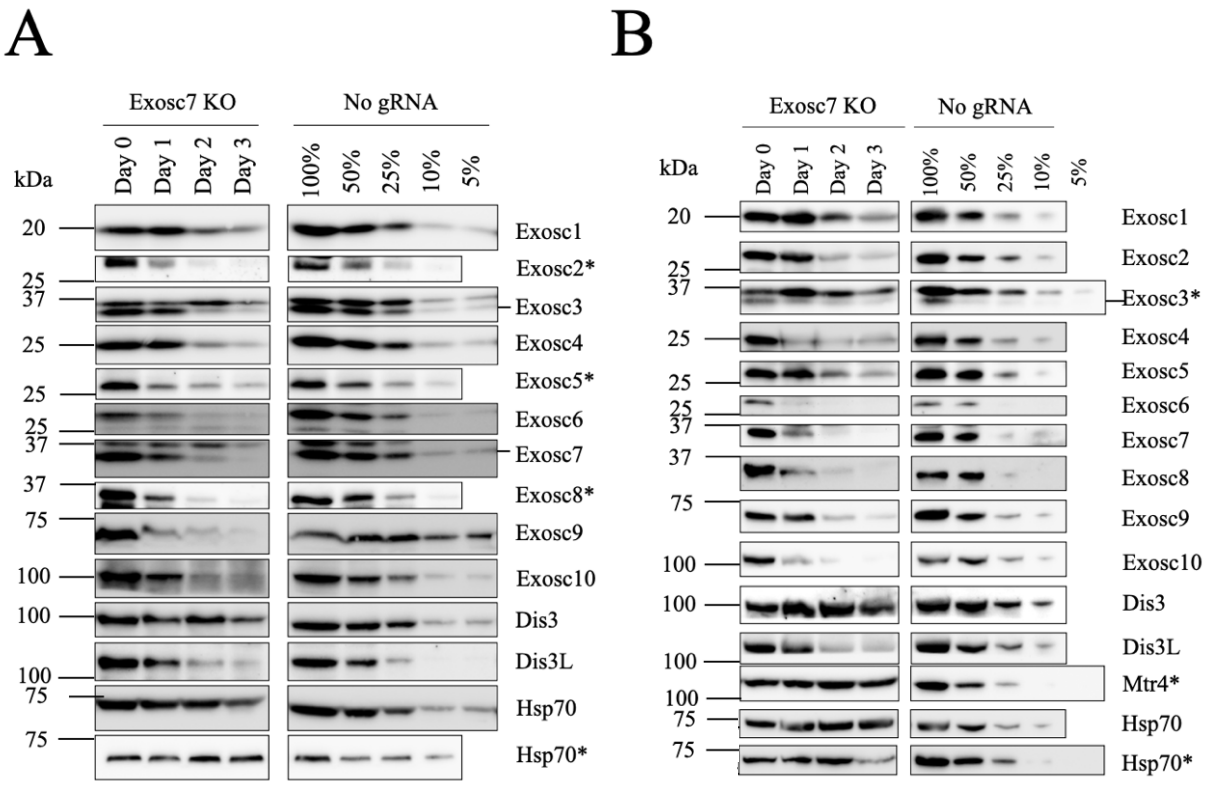

Supplementary Figure S8: Western blots of Exosc7 KO time courses, imaged to assess levels of exosome subunits. Asterisks indicate respective loading control. (**A**) Replicate 1. (**B**) Replicate 2, including nuclear helicase Mtr4.

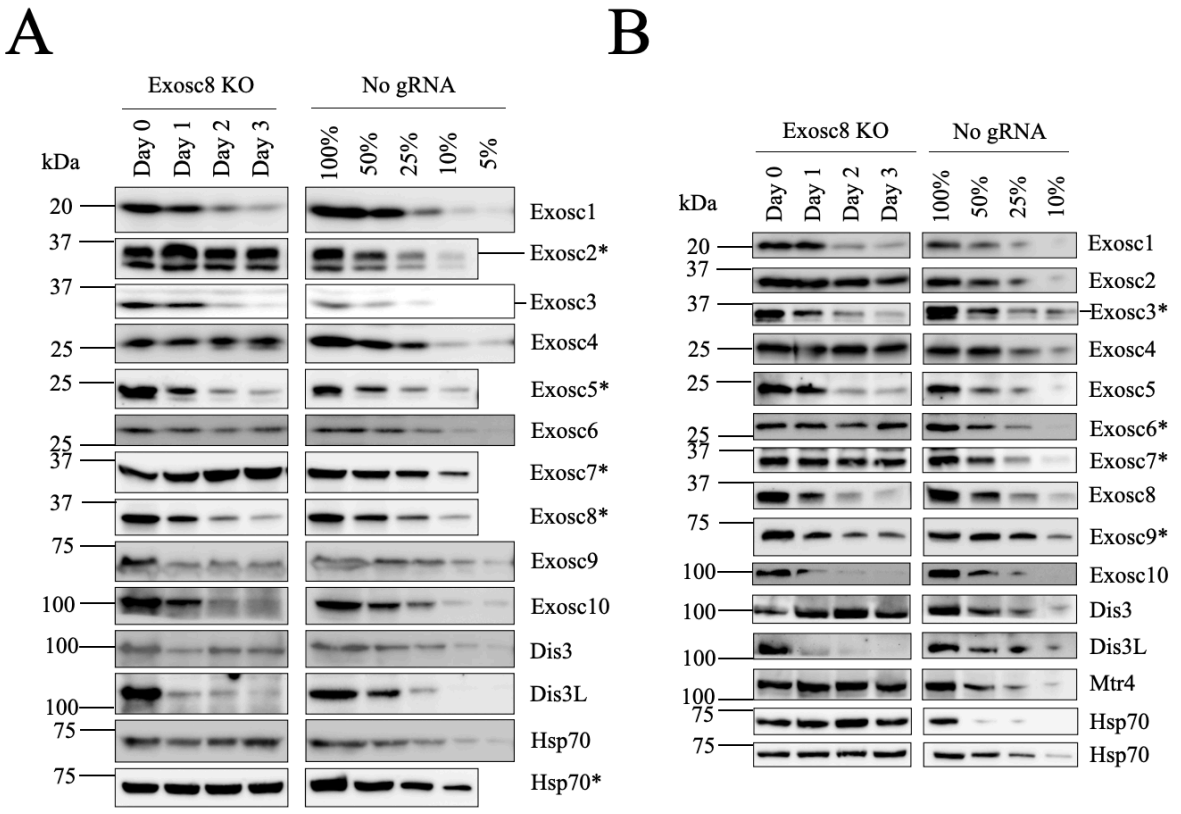

Supplementary Figure S9: Western blots of Exosc8 KO time courses, imaged to assess levels of exosome subunits. Asterisks indicate respective loading control. (**A**) Replicate 1. (**B**) Replicate 2, including nuclear helicase Mtr4. Different Exosc3 antibodies were used than in (A) to avoid unspecific band.

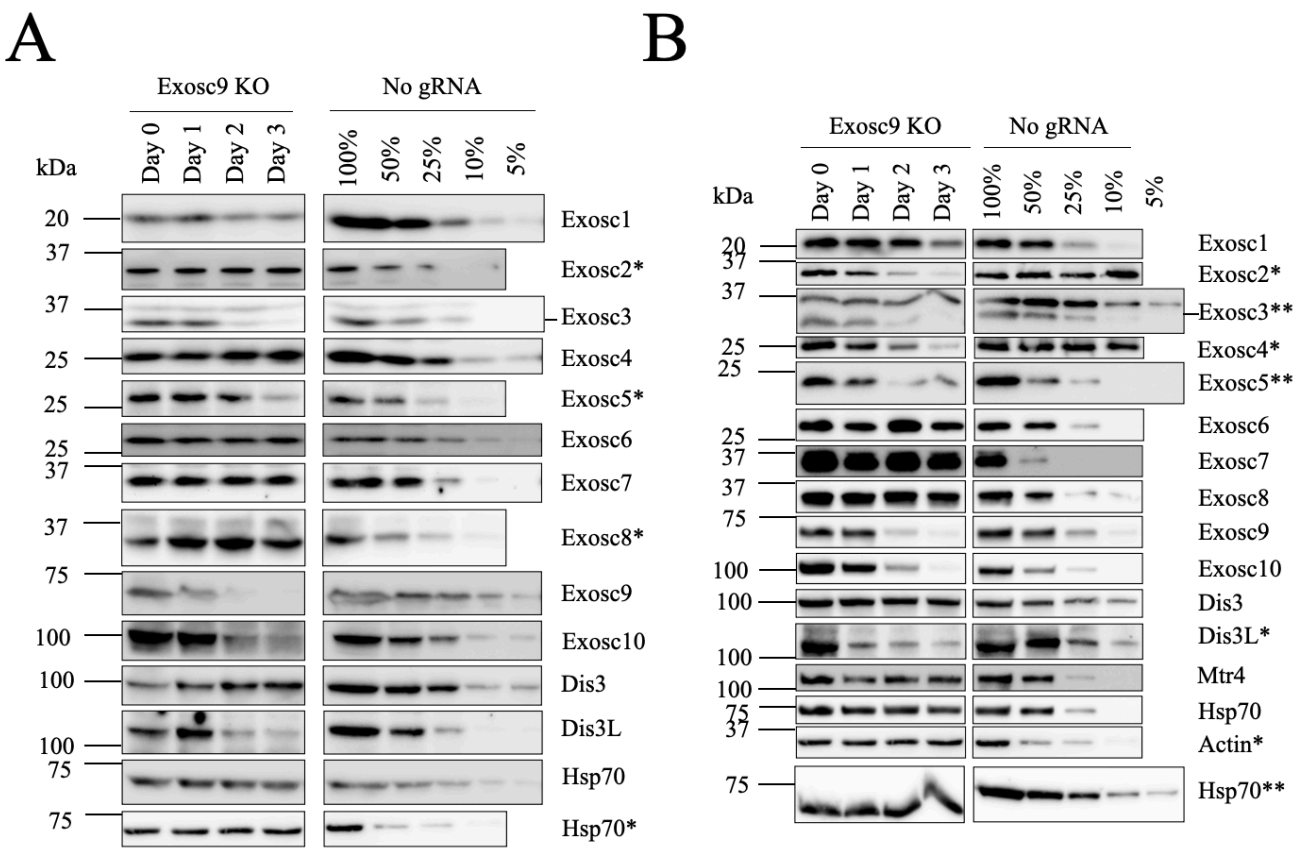

Supplementary Figure S10: Western blots of Exosc9 KO time courses, imaged to assess levels of exosome subunits. Asterisks indicate respective loading control. (**A**) Replicate 1. (**B**) Replicate 2, including nuclear helicase Mtr4.

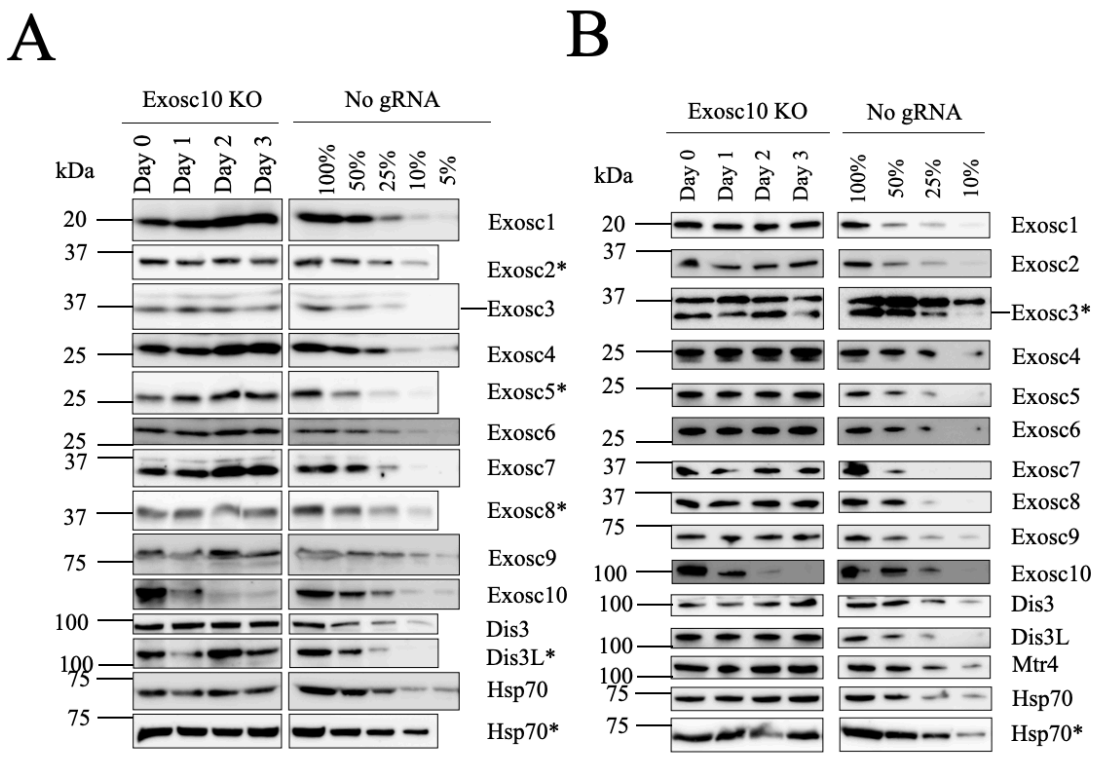

Supplementary Figure S11: Western blots of Exosc10 KO time courses, imaged to assess levels of exosome subunits. Asterisks indicate respective loading control. (**A**) Replicate 1. (**B**) Replicate 2, including nuclear helicase Mtr4.

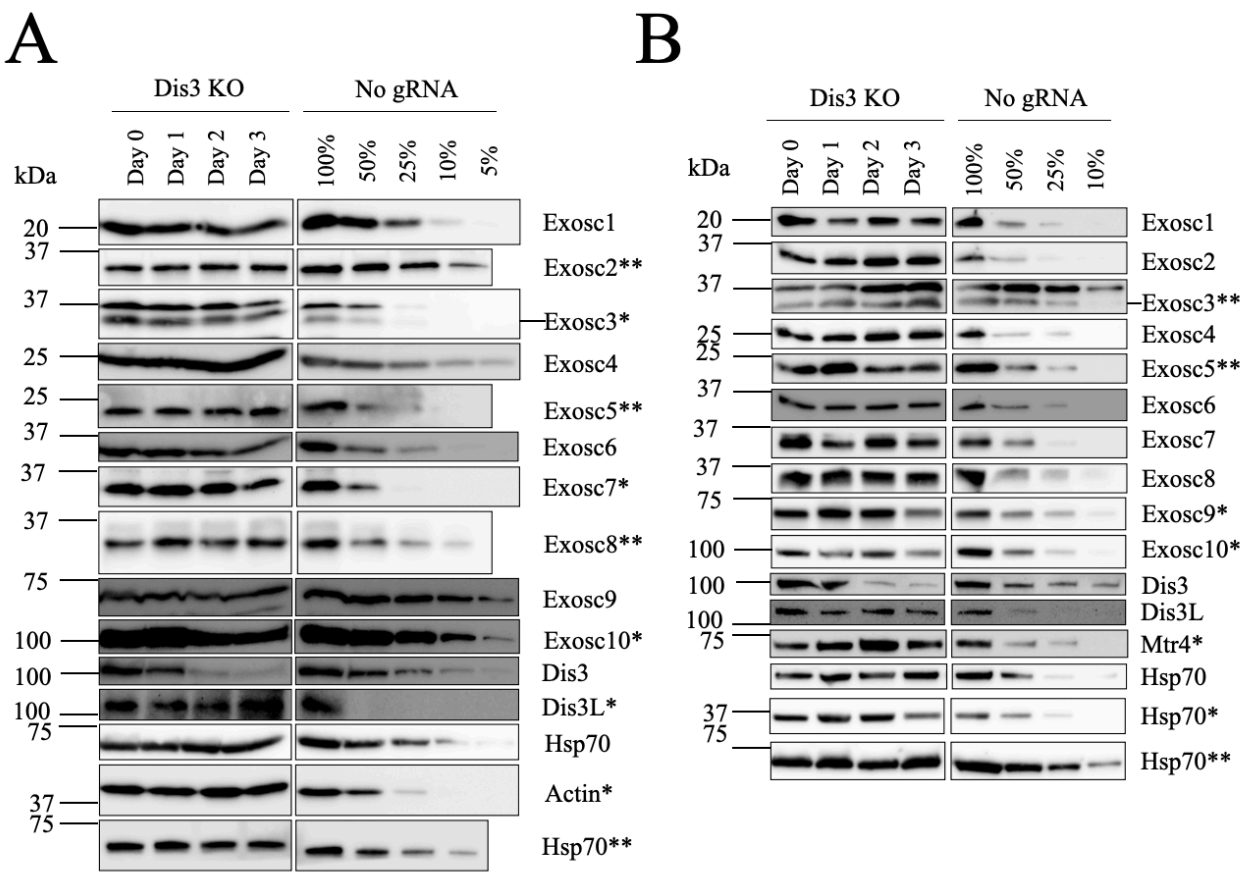

Supplementary Figure S12: Western blots of Dis3 KO time courses, imaged to assess levels of exosome subunits. Asterisks indicate respective loading control. (**A**) Replicate 1. (**B**) Replicate 2, including nuclear helicase Mtr4.

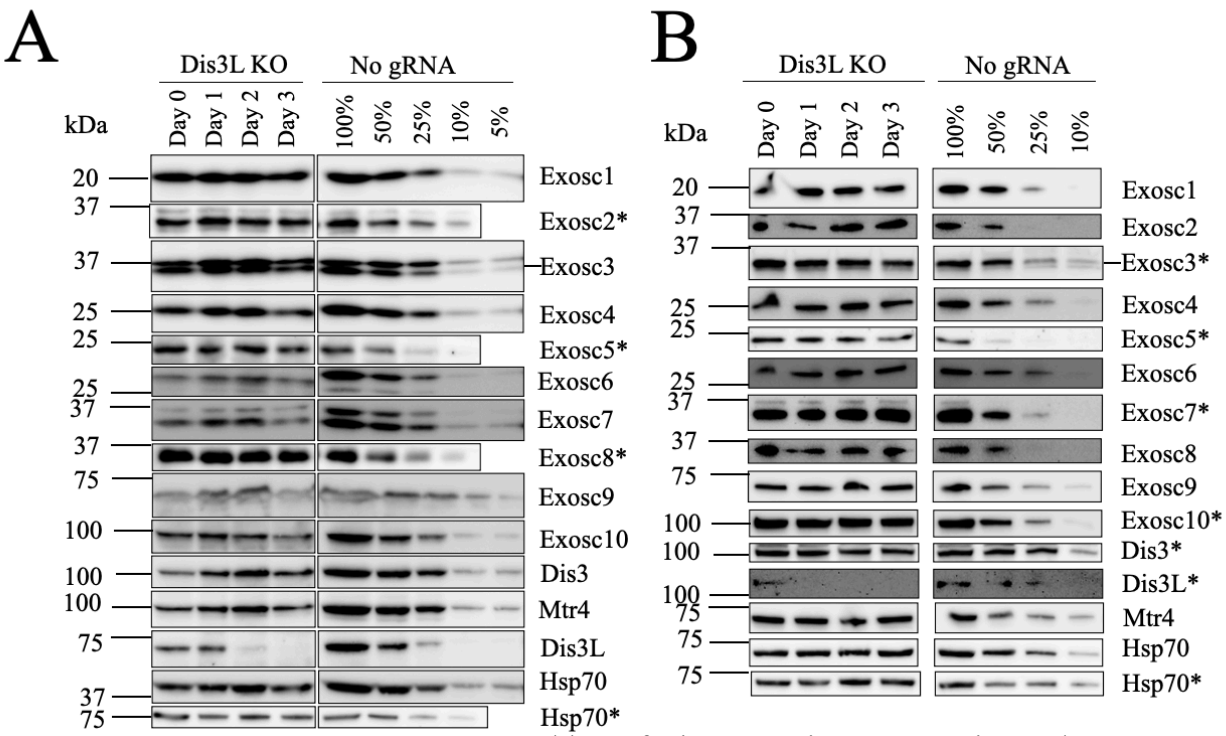

Supplementary Figure S13: Western blots of Dis3L KO time courses, imaged to assess levels of exosome subunits. (**A**) Replicate 1. (**B**) Replicate 2, including nuclear helicase Mtr4. Different Exosc3 antibodies were used than in (A) to avoid unspecific band.

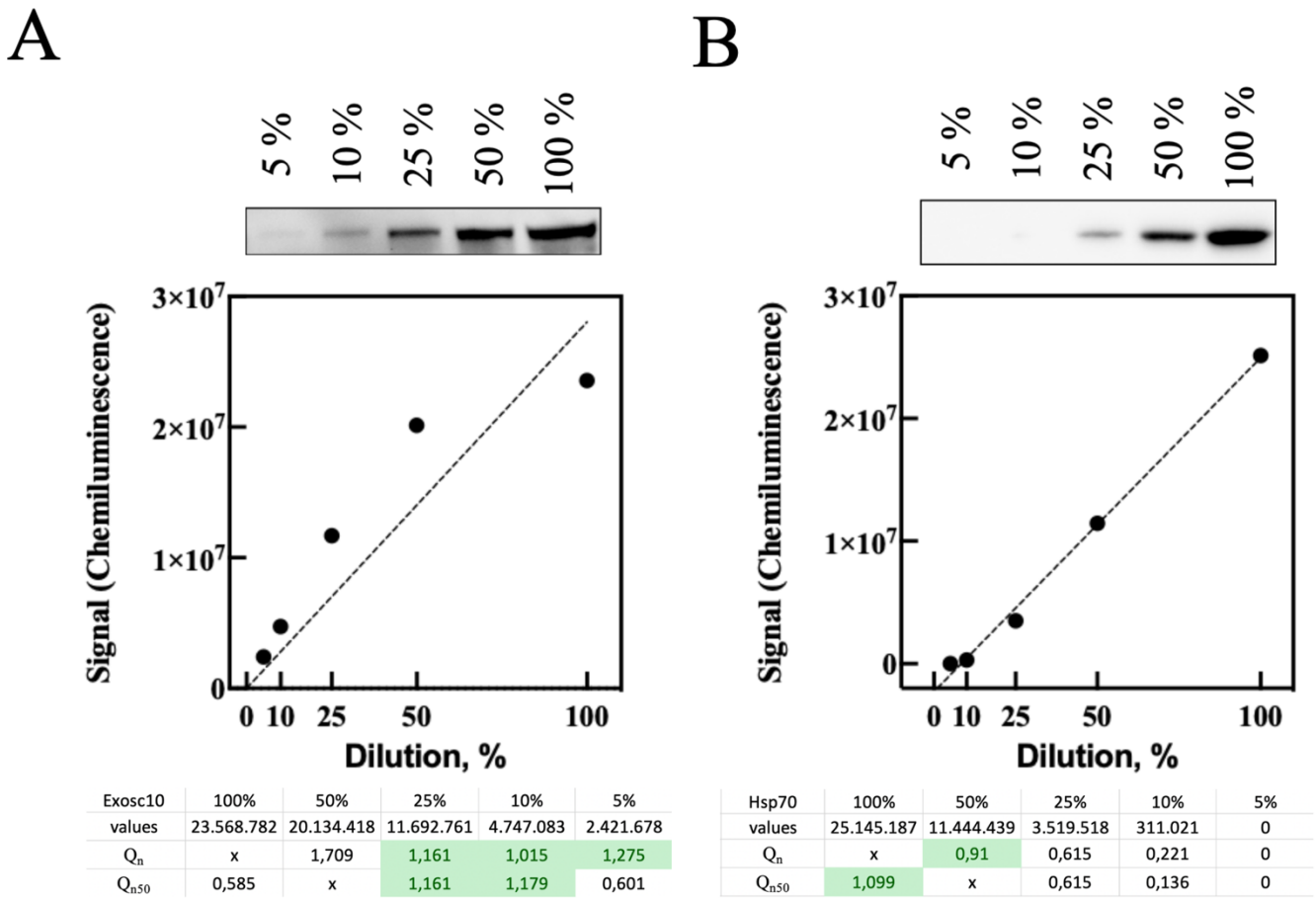

Exosc10	100%	50%	25%	10%	5%
values	23.568.782	20.134.418	11.692.761	4.747.083	2.421.678
Q_n	x	1,709	1,161	1,015	1,275
Q_{n50}	0,585	x	1,161	1,179	0,601

Hsp70	100%	50%	25%	10%	5%
values	25.145.187	11.444.439	3.519.518	311.021	0
Q_n	x	0,91	0,615	0,221	0
Q_{n50}	1,099	x	0,615	0,136	0

Supplementary Figure S14: (**A**) Dilution series of Exosc10 antibody from Exosc4 KO replicate 2 Western blots (Supplementary Fig. S5B), illustrating the loss of signal linearity in higher dilutions. On top is the Western blot, below the quantification and shown at the bottom are the background subtracted raw values and Q_n as well as Q_{n50}. (**B**) Dilution series of Hsp70 antibody from Exosc4 KO replicate 2 Western blots (Supplementary Fig. S5B), illustrating the loss of signal linearity at lower dilutions. On top is the Western blot, below the quantification and shown at the bottom are the background subtracted raw values and Q_n as well as Q_{n50}.